Available online at www.sciencedirect.com
SCIENCE DIRECT®
Physica D 197 (2004) 149–173
PHYSICA D
www.elsevier.com/locate/physd

Boundary-layer separation and adverse pressure gradient for 2-D viscous incompressible flow

Michael Ghil[a,b], Jian-Guo Liu[c], Cheng Wang[d], Shouhong Wang[e,*]

[a] *Département Terre-Atmosphére-océan, Erole Normale Supérieure, Paris, France*
[b] *Institute of Geophysics and Planetary Physics, University of California, Los Angeles, CA 90095, USA*
[c] *Department of Mathematics, Institute for Physical Science and Technology, University of Maryland, College Park, MD 20742-4015, USA*
[d] *Department of Mathematics, The University of Tennessee, Knoxville, TN 37996-1300, USA*
[e] *Department of Mathematics and Institute for Scientific Computing & Applied Mathematics, Indiana University, Rawles Hall, Bloomington, IN 47405-5701, USA*

Received 28 January 2004; received in revised form 2 June 2004; accepted 23 June 2004

Communicated by U. Frisch

Abstract

We study the detailed process of bifurcation in the flow's topological structure for a two-dimensional (2-D) incompressible flow subject to no-slip boundary conditions and its connection with boundary-layer separation. The boundary-layer separation theory of M. Ghil, T. Ma and S. Wang, based on the structural-bifurcation concept, is translated into vorticity form. The vorticity formulation of the theory shows that structural bifurcation occurs whenever a degenerate singular point for the vorticity appears on the boundary; this singular point is characterized by nonzero tangential second-order derivative and nonzero time derivative of the vorticity. Furthermore, we prove the presence of an adverse pressure gradient at the critical point, due to reversal in the direction of the pressure force with respect to the basic shear flow at this point. A numerical example of 2-D driven-cavity flow, governed by the Navier Stokes equations, is presented; boundary-layer separation occurs, the bifurcation criterion is satisfied, and an adverse pressure gradient is shown to be present.

MSC: 34D30; 35Q35; 65M06; 76D05; 76D10

Keywords: Divergence-free vector fields; Structural bifurcation; Navier–Stokes equations; Boundary layer separation; Adverse pressure gradient; Driven-cavity flow

* Corresponding author. Tel.: +1 812 855 8350; fax: +1 812 855 0046.
E-mail addresses: ghil@atmos.ucla.edu (M. Ghil); jliu@math.umd.edu (J.-G. Liu); wang@math.utk.edu (C. Wang); showang@indiana.edu (S. Wang)

0167-2780/$ – see front matter © 2004 Elsevier B.V. All rights reserved.
doi:10.1016/j.physd.2004.06.012

1. Introduction and outline of main results

The primary aim of this article is to investigate, theoretically as well as numerically, the topological aspects of boundary-layer separation in two-dimensional (2-D) incompressible flows. It is well-known that a boundary layer appears in any viscous incompressible flow, due to the slow-down of the flow by a no-slip boundary [13]. A shear flow is present in the transition area between the wall and the free fluid. The width of this shear layer, before the separation occurs, is proportional to $\sqrt{1/Re}$, where Re is the Reynolds number [29]. However, this shear layer can detach and separate from the boundary, generating vorticity and a recirculation area, which leads to the break-down of the monotone velocity profile in the boundary layer. Characterizing this separation is a long-standing problem in fluid mechanics, going back to the pioneering work of Prandtl [26].

The Prandtl equation is an asymptotic approximation of the Navier–Stokes equations within a thin layer near the boundary, which is only valid when no separation occurs. The mathematical analysis of the Prandtl equation up to date is reviewed in a recent book by Oleinik and Samokhin [24]. The book mainly deals with the regularity of the Prandtl equation when the pressure gradient along the boundary does not vanish. The blow-up of the Prandtl equation in finite time was established in [6]; this result, however, is not related to boundary-layer separation, which would render the equation invalid altogether. Some related work on this subject can also be found in [17,23,27,28,33,34].

It is observed experimentally that the point where the vorticity vanishes is a candidate for separation of the boundary layer. No known theorem, which can be applied to determine the separation point a priori, seems to have been available until the recent work of Ghil, Ma and Wang [10,11,19]. These authors developed a new theory to determine structural bifurcation of 2-D nondivergent vector fields $\boldsymbol{u} = \boldsymbol{u}(\boldsymbol{x}, t)$ near a so-called singular point $\boldsymbol{x}_0$ on the boundary ∂M of a compact manifold M, by analyzing the orbits of $\boldsymbol{u}$ near $\boldsymbol{x}_0$ and a critical transition time t_0. This ∂-singularity condition for $\boldsymbol{x}_0$ is related to the Prandtl condition for boundary-layer separation. It was shown that a 2-D incompressible velocity field $\boldsymbol{u}$ becomes structurally unstable, i.e., it changes its topological-equivalence class, if a ∂-singular point $\boldsymbol{x}_0$ on ∂M is degenerate. Such a point $\boldsymbol{x}_0$ corresponds precisely to a degenerate critical point for the scalar vorticity. This theory agrees with experimental observations, as well as with numerical simulations and physical reasoning.

The normal derivative of the velocity field $\partial \boldsymbol{u}/\partial \boldsymbol{n}$ has to satisfy the following sufficient criteria for structural bifurcation to occur: (1) a degenerate singular point $\boldsymbol{x}_0$ of $\partial \boldsymbol{u}/\partial \boldsymbol{n}$ appears on the boundary at the critical moment t_0; (2) one of the higher-order tangential derivatives of $\partial \boldsymbol{u}/\partial \boldsymbol{n}$ is nonzero; and (3) its time derivative is nonzero. The structural transition in the flow pattern predicted by these conditions gives rise to boundary-layer separation in the case that $\partial \boldsymbol{u}/\partial \boldsymbol{n}$ has a nonzero second-order derivative in the second condition, and the index of the shear field $\mathrm{ind}(\partial \boldsymbol{u}/\partial \boldsymbol{n}, \boldsymbol{x}_0)$ vanishes at the critical moment.

This result was obtained in [10] for the very general case in which $\boldsymbol{u}(\boldsymbol{x}, t)$ is a nondivergent vector field in 2-D, $\nabla \cdot \boldsymbol{u} = 0$, but the dependence on the parameter t is unspecified, except for the requirement that it be once continuously differentiable. The analysis in [10] was carried out for no-penetration, free-slip boundary conditions. A structural stability theorem for the same type of vector field, but with homogeneous Dirichlet boundary conditions, was proven by Ma and Wang [19]. The structural bifurcation result quoted above was obtained for Dirichlet boundary conditions in [11]. It is the latter result that corresponds to boundary-layer separation and will be used in the present paper.

The theory developed in [10,11,19] is recapitulated in Section 2. In Section 3, the above conditions in velocity form are translated into vorticity form. Naturally, the previous conclusion for the bifurcation is still valid under the same set of the conditions, put into this vorticity form. This is the first part of our analytical result here, which is stated as Theorem 3.2. An application of the maximum principle for subharmonic functions yields the presence of an adverse pressure gradient in the tangential direction along the boundary near the isolated singular point and the critical transition time. This is the second part of Theorem 3.2.

More precisely, we consider 2-D viscous incompressible flows described by the Navier–Stokes equations. An incompressible solution of these equations can be viewed as a one-parameter family of divergence-free vector fields with time t as the parameter. We show in Section 3 that an adverse pressure gradient is present near the critical

point P^* and the critical moment T^* of boundary-layer separation, which correspond to $\boldsymbol{x}_0$ and t_0 in the analysis of Section 2. Under the above conditions, the vorticity reaches a local extremum in space and, according to whether this extremum is a maximum or a minimum, it decreases or increases in time. Applying the vorticity transport equation near the boundary point P^* and using no-slip boundary conditions for the velocity field shows that the vorticity field is subharmonic or superharmonic in a small neighborhood of P^*. Since the critical point P^* is also a spatially local extremum for the vorticity, we conclude from the Hopf Lemma that the vorticity gradient is directed outward or inward there. Thus the presence of an adverse pressure gradient follows directly from the fact that the tangential derivative of the pressure is exactly the normal derivative of the vorticity, which can be seen by applying the original Navier–Stokes equations near the boundary. The combination of these results provides an explanation for the mechanism of boundary-layer separation, in a rigorous mathematical context.

A numerical example of driven-cavity flow is presented in Section 4 to illustrate the structural bifurcation of 2-D incompressible flow associated with boundary-layer separation. No-slip boundary conditions are imposed on the left, right and bottom boundary sections, while a parabolic velocity profile is imposed on the top boundary, with the velocity vector parallel to this boundary section and pointing to the right. The cavity flow is computed as the solution of the 2-D incompressible Navier–Stokes equations with the prescribed Dirichlet boundary conditions. An Essentially Compact Fourth-Order Scheme (EC4) [8,31,32] is applied to solve the equations on a high-resolution grid of $(N+1)\times(N+1)$ points, with increasing values of $N = 1024$, 1536 and 2048. The Reynolds number is taken to be $Re = 10^5$ and the flow behavior with respect to boundary-layer separation near the mid-point of the right boundary is investigated in detail.

A thin boundary layer forms due to the combination of the no-slip boundary condition and the basic circulation in the cavity. The vorticity field stays positive initially throughout the boundary layer. As time goes on, if a degenerate singular point for the vorticity, with positive second-order tangential derivative and negative time derivative, appears on the right boundary, structural transition is assured to happen and the boundary layer separates.

The numerical solution shows the detailed process of the flow's structural bifurcation and boundary-layer separation, including the accurate location of the degenerate singular points for the vorticity, the first and second critical time, and the fine details of the flow in the recirculation area. The zoom plot of the vorticity near the bifurcation point exhibits a negative normal derivative, which indicates a reverse pressure gradient at that point. This numerical result matches the analytical argument in Section 3. Zoom plots of the vortex shedding after the structural bifurcation are also presented. Section 4 concludes with a discussion of the way that the separated and rolled-up boundary layer interacts with the flow in the interior of the rectangular cavity.

The theory presented here is restricted to 2-D cases. The analysis for the kinematic theory, as well as the connections to dynamics in three-dimensional (3-D) cases are still wide open. It is clear that the classical notion of structural stability does not appear to be applicable, and the full classification of 3-D divergence-free vector fields is not within immediate reach: it is quite difficult to classify bifurcations and transitions of 3-D flow structures in general. Large-scale, planetary flows, atmospheric and oceanic, however, are characterized by fast rotation (small Rossby number) and strong stratification (small vertical-to-horizontal aspect ratio), at least in the midlatitudes; see Ghil and Childress [9] and Pedlosky [25]. It is expected that progress can be made for such geophysical flows modeled by the 3-D baroclinic quasi-geostrophic equations. Likewise, generalizations of the present theory might be possible for 3-D axis-symmetric flows, which possess a so-called Stokes stream function [1].

2. Recapitulation of structural bifurcation in 2-D flows

In this section, we recall the key concepts and results of the structural bifurcation theory developed recently by Ghil, Ma and Wang [10,11,19]. This theory provides a full classification of the topological structure of 2-D nondivergent vector fields on a compact manifold with boundary, subject to either no-penetration or Dirichlet boundary conditions, along with the conditions for transition from one topological class to another. As a by-product, this theory gives a rigorous characterization of boundary-layer separation of 2-D incompressible fluid flows.

For simplicity, we treat here the Euclidean case, but a piece of a sphere S^2 is also covered by the general theory of [10,11,19]. So, let $M \subset \mathbb{R}^2$ be a closed and bounded domain with a sufficiently smooth boundary $\partial M \in C^{r+1}(r \geq 2)$, and TM be the tangent bundle of M. Let $C_n^r(TM)$ be the space of all C^r vector fields on M with the no-penetration boundary condition, $D^r(TM)$ the subspace of $C_n^r(TM)$ that is divergence-free, and $B_0^r(TM)$ the subspace of $D^r(TM)$ that satisfies homogeneous Dirichlet boundary conditions:

$$
\begin{aligned}
C_n^r(TM) &= \{\boldsymbol{u} \in C^r(TM) \quad |\boldsymbol{u}_n|_{\partial M} = 0\},\\
D^r(TM) &= \{\boldsymbol{u} \in C^r(TM) \quad |\boldsymbol{u}_n|_{\partial M} = 0, \operatorname{div} \boldsymbol{u} = 0\},\\
B_0^r(TM) &= \{\boldsymbol{u} \in D^r(TM) \quad |\boldsymbol{u}|_{\partial M} = 0\}.
\end{aligned}
$$

Here, $\boldsymbol{u}_n = \boldsymbol{u} \cdot \boldsymbol{n}$ and $\boldsymbol{u}_\tau = \boldsymbol{u} \cdot \tau$, where $\boldsymbol{n}$ and τ are the unit normal and tangent vectors on ∂M, respectively. It is easy to see that

$$B_0^r(TM) \subset D^r(TM) \subset C_n^r(TM) \subset C^r(TM).$$

We start with some basic concepts. Let $X = D^r(TM)$ or $B_0^r(TM)$ in the following definitions.

Definition 2.1. Two vector fields $\boldsymbol{u}, \boldsymbol{v} \in D^r(TM)$ are called topologically equivalent if there exists a homeomorphism of $\varphi : M \to M$, which takes the orbits of $\boldsymbol{u}$ to orbits of $\boldsymbol{v}$ and preserves their orientation.

Definition 2.2. Let $\boldsymbol{u} \in C^1([0, T], X)$. The vector field $\boldsymbol{u}_0 = \boldsymbol{u}(\cdot, t_0)$ $(0 < t_0 < T)$ is called a bifurcation point of $\boldsymbol{u}$ at the parameter value $t = t_0$ if, for any $t^- < t_0$ and $t_0 < t^+$ with t^- and t^+ sufficiently close to t_0, the vector field $\boldsymbol{u}(\cdot; t^-)$ is not topologically equivalent to $\boldsymbol{u}(\cdot; t^+)$. In this case, we say that $\boldsymbol{u}(\boldsymbol{x}, t)$ has a bifurcation at t_0 in its global structure.

Definition 2.3. Let $\boldsymbol{u} \in C^1([0, T], X)$. We say that $\boldsymbol{u}(x, t)$ has a bifurcation in its local structure in a neighborhood $U \subset M$ of $\boldsymbol{x}_0$ at the parameter value $t = t_0 (0 < t_0 < T)$ if, for any $t^- < t_0$ and $t_0 < t^+$ with t^- and t^+ sufficiently close to t_0, the vector fields $\boldsymbol{u}(\cdot; t^-)$ and $\boldsymbol{u}(\cdot; t^+)$ are not topologically equivalent locally in $U \subset M$.

The difference between bifurcation in local vs. global structure is further clarified in Fig. 1 of [11].

Definition 2.4. A vector field $\boldsymbol{v} \in X$ is called structurally stable in X if there exists a neighborhood $\mathcal{O} \subset X$ of $\boldsymbol{v}$ such that for any $\boldsymbol{u} \in \mathcal{O}$, $\boldsymbol{u}$ and $\boldsymbol{v}$ are topologically equivalent.

We recall next some basic facts and definitions on divergence-free vector fields. Let $\boldsymbol{v} \in D^r(TM)$.

(1) A point $p \in M$ is called a *singular point* of $\boldsymbol{v}$ if $\boldsymbol{v}(p) = 0$; a singular point p of $\boldsymbol{v}$ is called *non-degenerate* if the Jacobian matrix $D\boldsymbol{v}(p)$ is invertible; $\boldsymbol{v}$ is called *regular* if all singular points of $\boldsymbol{v}$ are non-degenerate.
(2) An interior non-degenerate singular point of $\boldsymbol{v}$ can be either a center or a saddle, and a non-degenerate boundary singularity must be a saddle.
(3) Saddles of $\boldsymbol{v}$ must be connected to saddles. An interior saddle $p \in M$ is called *self-connected* if p is connected only to itself, i.e. p occurs in a graph whose topological form is that of the number 8.
(4) The vector field $\boldsymbol{v}$ is structurally stable near each of its non-degenerate singular points.

When $\boldsymbol{u} \in B_0^r(TM)$, $r \geq 2$, a different singularity concept was introduced for points on the boundary in [19]. We recall it as follows.

(1) A point $p \in \partial M$ is called a *∂-regular point* of $\boldsymbol{u}$ if $\partial \boldsymbol{u}_\tau(p)/\partial \boldsymbol{n} \neq 0$; otherwise, $p \in \partial M$ is called a *∂-singular point* of $\boldsymbol{u}$.
(2) A ∂-singular point $p \in \partial M$ of $\boldsymbol{u}$ is called *non-degenerate* if

$$\det \begin{pmatrix} \dfrac{\partial^2 \boldsymbol{u}_\tau(p)}{\partial \tau \partial \boldsymbol{n}} & \dfrac{\partial^2 \boldsymbol{u}_\tau(p)}{\partial \boldsymbol{n}^2} \\ \dfrac{\partial^2 \boldsymbol{u}_n(p)}{\partial \tau \partial \boldsymbol{n}} & \dfrac{\partial^2 \boldsymbol{u}_n(p)}{\partial \boldsymbol{n}^2} \end{pmatrix} \neq 0.$$

A non-degenerate ∂-singular point of $\boldsymbol{u}$ is also called a *∂-saddle point* of $\boldsymbol{u}$.
(3) A vector $\boldsymbol{u} \in B_0^r(TM)$ $(r \geq 2)$ is called *D*-regular if $\boldsymbol{u}$ is regular in the interior M°, and all ∂-singular points of $\boldsymbol{u}$ on ∂M are non-degenerate.

The following theorem of T. Ma and S. Wang in [19] provides necessary and sufficient conditions for structural stability of a divergence-free vector field.

Theorem 2.5 (Ma and Wang [19]). *Let $\boldsymbol{u} \in B_0^r(TM)(r \geq 2)$. Then $\boldsymbol{u}$ is structurally stable in $B_0^r(TM)$ if and only if*

(1) $\boldsymbol{u}$ is *D-regular*;
(2) *all interior saddle points of $\boldsymbol{u}$ are self-connected*; *and*
(3) *each ∂-saddle point of $\boldsymbol{u}$ on ∂M is connected to a ∂-saddle point on the same connected component of ∂M.*

Moreover, the set of all structurally stable vector fields is open and dense in $B_0^r(TM)$.

Next, we recall the definition of indices of singular points of a vector field [22]. Let $p \in M$ be an isolated singular point of $\boldsymbol{v} \in C_n^r(TM)$; then

$$\mathrm{ind}(\boldsymbol{v}, p) = \deg(\boldsymbol{v}, p),$$

where $\deg(\boldsymbol{v}, p)$ is the Brouwer degree of $\boldsymbol{v}$ at p.

Let $p \in \partial M$ be an isolated singular point of $\boldsymbol{v}$, and $\tilde{M} \subset \mathbb{R}^2$ be an extension of M, i.e. $M \subset \tilde{M}$ such that $p \in \tilde{M}$ is an interior point of $\tilde{M}$. In a neighborhood of p in $\tilde{M}$, $\boldsymbol{v}$ can be extended by reflection to $\tilde{\boldsymbol{v}}$ such that p is an interior singular point of $\tilde{\boldsymbol{v}}$, thanks to the no-penetration condition $\boldsymbol{v} \cdot \boldsymbol{n}|_{\partial M} = 0$. Then we define the index of $\boldsymbol{v}$ at $p \in \partial M$ by

$$\mathrm{ind}(\boldsymbol{v}, p) = \tfrac{1}{2}\mathrm{ind}(\tilde{\boldsymbol{v}}, p).$$

Let $p \in M$ be an isolated singular point of $\boldsymbol{v} \in C^r(TM)$. An orbit γ of $\boldsymbol{v}$ is said to be a stable orbit (resp. an unstable orbit) connected to p, if the limit set $\omega(\boldsymbol{x}) = p$ (resp. $\alpha(\boldsymbol{x}) = p$) for any $\boldsymbol{x} \in \gamma$; here $\omega(\boldsymbol{x})$ and $\alpha(\boldsymbol{x})$ are the forward and backward limit sets of $\boldsymbol{x}$, respectively.

We now recall a singularity classification theorem for 2-D nondivergent vector fields, which will be useful in our discussion of structural bifurcation.

Theorem 2.6 (Singularity Classification Theorem [10]). *Let M be a 2-D compact manifold with or without boundary, and $p \in M$ be an isolated singular point of $\boldsymbol{u} \in D^r(TM)$, $r \geq 1$. Then p is connected only to a finite number of orbits and the stable and unstable orbits connected to p alternate when tracing a closed curve around p. Furthermore,*

(1) *if $p \in M^\circ$, then p is connected by $2n$ $(n \geq 0)$ orbits, n of which are stable, and the other n unstable, while the index of $\boldsymbol{u}$ at p is*:

$$\mathrm{ind}(\boldsymbol{u}, p) = 1 - n;$$

(2) *if $p \in \partial M$, then p is connected by $n+2$ ($n \geq 0$) orbits, two of which are on the boundary ∂M, and the index of p is*:

$$\mathrm{ind}(\boldsymbol{u}, p) = -\tfrac{1}{2}n.$$

For simplicity, we assume here that the boundary ∂M contains a flat part $\Gamma \subset \partial M$ and consider structural bifurcation near a ∂-singular point $\boldsymbol{x}_0 \in \Gamma$. In such a case, a coordinate system (x_1, x_2) can be chosen such that $\boldsymbol{x}_0 = (x_0, 0)$ and Γ be given by

$$\Gamma = \{(x_1, 0) \mid |x_1 - x_0| \leq \delta\},$$

for some $\delta > 0$.

Next let $\boldsymbol{u}, \boldsymbol{v} \in C^1([0, T], B_0^r(TM))$ be Taylor expanded as:

$$\begin{cases} \boldsymbol{u}(\boldsymbol{x}, t) = \boldsymbol{u}^0(\boldsymbol{x}) + (t - t_0)\boldsymbol{u}^1(\boldsymbol{x}) + \mathrm{O}(|t - t_0|), \\ \boldsymbol{v}(\boldsymbol{x}, t) = \boldsymbol{v}^0(\boldsymbol{x}) + (t - t_0)\boldsymbol{v}^1(\boldsymbol{x}) + \mathrm{O}(|t - t_0|), \\ \boldsymbol{u}^0(\boldsymbol{x}) = \boldsymbol{u}(\boldsymbol{x}, t_0), \quad \boldsymbol{u}^1(\boldsymbol{x}) = \dfrac{\partial \boldsymbol{u}(\boldsymbol{x}, t)}{\partial t}\Big|_{t=t_0}, \\ \boldsymbol{v}^0(\boldsymbol{x}) = \dfrac{\partial \boldsymbol{u}^0}{\partial \boldsymbol{n}}, \quad \boldsymbol{v}^1(\boldsymbol{x}) = \dfrac{\partial \boldsymbol{u}^1}{\partial \boldsymbol{n}}. \end{cases} \tag{2.1}$$

Before we state the main result, we make the following assumption.

Assumption (H). There exists an isolated, ∂-singular point $\boldsymbol{x}_0 \in \partial M$ of $\boldsymbol{v}^0$ and an integer $k \geq 2$ such that $\boldsymbol{v}^0, \boldsymbol{v}^1 \in C^{k+1}$ near the point $\boldsymbol{x}_0$, and

$$\boldsymbol{v}^0(\boldsymbol{x}_0) = 0 \quad \text{(Prandtl condition)} \tag{2.2}$$

$$\mathrm{ind}(\boldsymbol{v}^0, \boldsymbol{x}_0) \neq -\tfrac{1}{2} \quad \text{(first necessary condition)} \tag{2.3}$$

$$\boldsymbol{v}^1(\boldsymbol{x}_0) \neq 0 \quad \text{(second necessary condition)} \tag{2.4}$$

$$\frac{\partial^k(\boldsymbol{v}_\tau^0(\boldsymbol{x}_0))}{\partial \tau^k} \neq 0 \quad \text{(technical condition)}. \tag{2.5}$$

Under Assumption (H), the flow structure of $\boldsymbol{u}$ near $\boldsymbol{x}_0$ and t_0 is fully classified in [10,11] and structural bifurcation is shown to occur at $\boldsymbol{x}_0$, as t crosses t_0.

Theorem 2.7 ([11]). *Let $\boldsymbol{u} \in C^1([0, T], B_0^r(TM))$ ($r \geq 2$) satisfy* Assumption (H). *Then there exists a neighborhood $\Gamma_0 \subset \partial M$ of $\boldsymbol{x}_0$ and an $\epsilon_0 > 0$ such that all ∂-singular points of $\boldsymbol{u}(\boldsymbol{x}, t \pm \varepsilon)$ in Γ^0 are non-degenerate for any $0 < \varepsilon \leq \epsilon_0$. Moreover,*

(1) *if the index* $\mathrm{ind}(\boldsymbol{v}^0, \boldsymbol{x}_0)$ *is an integer, then one of $\boldsymbol{u}(\boldsymbol{x}, t_0 \pm \varepsilon)$ has two ∂-singular points on Γ_0, and the other one has no ∂-singular point on Γ_0; and*
(2) *if the index* $\mathrm{ind}(\boldsymbol{v}^0, \boldsymbol{x}_0)$ *is not an integer, then each of $\boldsymbol{u}(\boldsymbol{x}, t_0 \pm \varepsilon)$ has only one ∂-singular point on Γ_0.*

Theorem 2.8 (Structural bifurcation theorem [11]). *Let $\boldsymbol{u} \in C^1([0, T], B_0^r(TM))(r \geq 2)$ satisfy* Assumption (H). *Then*

(1) *$\boldsymbol{u}(\boldsymbol{x}, t)$ has a bifurcation in its local structure at $(\boldsymbol{x}_0, t_0)$; and*
(2) *if $\boldsymbol{x}_0 \in \partial M$ is a unique singular point which has the same index as* $\mathrm{ind}(\boldsymbol{v}^0, \boldsymbol{x}_0)$ *on ∂M, then $\boldsymbol{u}(\boldsymbol{x}, t)$ has a bifurcation in its global structure at $t = t_0$.*

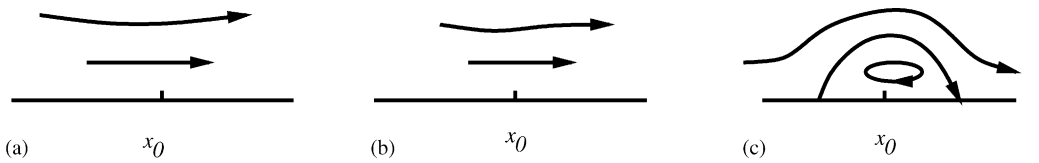

Fig. 1. Structural bifurcation for $\mathrm{ind}(\boldsymbol{v}^0, \boldsymbol{x}_0) = 0$.

In the case where $\mathrm{ind}(\boldsymbol{v}^0, \boldsymbol{x}_0) = 0$, the above structural bifurcation theorem corresponds to boundary-layer separation in 2-D incompressible flows, as outlined in Section 1. Here, $\boldsymbol{u}^0$ is given by Fig. 1(b). For a sufficiently small $\varepsilon > 0$, $\boldsymbol{u}(\boldsymbol{x}, t_0 - \varepsilon)$ given by Fig. 1(a) has no singular points near $\boldsymbol{x}_0$. On the other hand, $\boldsymbol{u}(\boldsymbol{x}, t_0 + \varepsilon)$ given by Fig. 1(c) has two singular points near $\boldsymbol{x}_0$ on the boundary and one center near $\boldsymbol{x}_0$ in the interior, all of which are non-degenerate.

The analysis is delicate and was done first for the case with boundary conditions of no normal flow [10], and then for the case with homogeneous Dirichlet boundary conditions [11,19].

3. Adverse pressure gradient at the separation point

In this section, we show the existence of an adverse pressure gradient in the neighborhood of the bifurcation point $(\boldsymbol{x}_0, t_0)$ by utilizing the relation between the vorticity and pressure in the solutions of the Navier–Stokes equations and applying the Hopf Lemma [12] for subharmonic functions. We use the 2-D Navier–Stokes equations in the incompressible form

$$\begin{cases} \partial_t \boldsymbol{u} + (\boldsymbol{u} \cdot \nabla)\boldsymbol{u} + \nabla p = \frac{1}{Re}\Delta \boldsymbol{u}, \\ \nabla \cdot \boldsymbol{u} = 0, \end{cases} \tag{3.1}$$

with the no-slip boundary conditions:

$$\boldsymbol{u} = 0, \quad \text{on } \partial M. \tag{3.2}$$

In the system (3.1)–(3.2), $\boldsymbol{u} = (u, v)$ is the velocity, p the pressure, and Re the Reynolds number. For simplicity we let $\nu = 1/Re$. The solutions of this system can be viewed as one-parameter families of divergence-free vector fields with the time t as the parameter. Hence, the analysis reviewed in Section 2 can be applied to such a solution. For such a family of divergence-free vector fields $\boldsymbol{u}(t)$, structural bifurcation, i.e., change in topological equivalence class, occurs at T^* if the normal derivative of the velocity field $\boldsymbol{u_n} = \partial \boldsymbol{u}/\partial \boldsymbol{n}$ has a degenerate singular point $P^* \in \partial M$ such that $\partial \boldsymbol{u_n}/\partial t$ is nonzero. Note that T^*, $\boldsymbol{u_n}$, and $P^* \in \partial M$ correspond to t_0, the vector field $\boldsymbol{v}^0$ and $\boldsymbol{x}_0 \in \partial M$ in Section 2, respectively.

The connection between the structural bifurcation analysis and the solution of the incompressible Navier–Stokes Eqs. (3.1) and (3.2) is made through the introduction of the vorticity $\omega = \nabla \times \boldsymbol{u} = -\partial_y u + \partial_x v$. Applying the curl operator $\nabla\times$ to the momentum Eq. (3.1) gives a transport equation for the scalar field ω:

$$\partial_t \omega + (\boldsymbol{u} \cdot \nabla)\omega = \nu \Delta \omega. \tag{3.3}$$

Numerical simulations, like the one given in Section 4 below, as well as laboratory experiments, show that the formation of recirculating cells starts at the moment when the vorticity reaches its zero point on the boundary as a local maximum (minimum) point in space and decreases (increases) in time. That point is known as the separation point and we denote it as $P^* \in \partial M$ at the moment $t = T^*$. For simplicity of presentation and in agreement with the numerical example in Section 4, we assume that a section of the vertical line $x = 1$, which is denoted by

Γ^0, is included in ∂M and that P^* lies on the boundary section Γ^0. The unit normal and tangential vectors on Γ^0 are $\boldsymbol{n} = (1, 0)$, $\tau = (0, 1)$, respectively; this determines the normal and tangential derivatives to be $\partial/\partial \boldsymbol{n} = \partial_x$, $\partial/\partial\tau = \partial_y$.

In the boundary layer, pure shear flow occurs along the boundary section Γ^0 before the critical time T^*. Without loss of generality and for the sake of consistency with the numerical example in Section 4, it is assumed that this shear flow is downward, i.e., toward negative y-values. Mathematically speaking, this amounts to assuming that there exists a neighborhood $\boldsymbol{U}_1$ of P^* such that the boundary of $\boldsymbol{U}_1$ includes a portion of Γ^0 and

$$\omega \geq 0 \quad \text{in} \quad \boldsymbol{U}_1, \ \text{when} \quad t < T^*. \tag{3.4}$$

This condition implies that the vorticity reaches zero at (P^*, T^*) as a local minimum in space and decreases afterward in time. In this case, the formation of a recirculating flow region is given by the following conditions

$$\omega(P^*, T^*) = 0, \qquad \frac{\partial\omega}{\partial\tau}(P^*, T^*) = 0, \qquad \frac{\partial^2\omega}{\partial\tau^2}(P^*, T^*) > 0, \qquad \frac{\partial\omega}{\partial t}(P^*, T^*) < 0. \tag{3.5}$$

In fact, we have the following proposition connecting (3.5) to Assumption (H); the proof of this proposition will be given at the end of the present section.

Proposition 3.1.

(1) Assumption (H) *with* $k = 2$ *for the velocity field* $\boldsymbol{u}$ *is equivalent to the following conditions on the vorticity* ω:

$$\omega(P^*, T^*) = 0, \qquad \frac{\partial\omega}{\partial\tau}(P^*, T^*) = 0, \qquad \frac{\partial^2\omega}{\partial\tau^2}(P^*, T^*) \neq 0, \qquad \frac{\partial\omega}{\partial t}(P^*, T^*) \neq 0. \tag{3.6}$$

(2) *If* (3.4) *holds true, i.e., only downward shear flow is present around* Γ^0 *for* $t < T^*$, Assumption (H) *is equivalent to* (3.5).

The main result of this section is the following theorem, showing the existence of an adverse pressure gradient at the separation point.

Theorem 3.2. *Let* $(\boldsymbol{u}, p)$ *be the solution of the 2-D Navier–Stokes equations* (3.1) *with boundary conditions* (3.2). *Assume that there exist a boundary point* $P^* \in \partial M$ *and a critical time* T^* *such that* (3.4) *and* (3.5) *hold true. Then*

(1) *structural bifurcation occurs in the local structure of* $\boldsymbol{u}$ *at the boundary point* P^* *as* t *crosses* T^*, *and boundary-layer separation evolves exactly as shown in Fig. 1*; *and*
(2) *an adverse pressure gradient in the tangent direction is present at* P^*, *i.e.*,

$$\frac{\partial p}{\partial\tau} = \frac{\partial p}{\partial y} < 0, \quad \text{at} \quad (P^*, T^*). \tag{3.7}$$

Proof of Theorem 3.2. The first part is a direct consequence of Proposition 3.1 here and of Theorem 2.8 in Section 2. For the second part, we see that the vorticity transport Eq. (3.3) at the boundary point P^* gives

$$\Delta\omega = \frac{1}{\nu}(\partial_t\omega + (\boldsymbol{u}\cdot\nabla)\omega) = \nu^{-1}\partial_t\omega < 0, \quad \text{at } (P^*, T^*). \tag{3.8}$$

The second equality in (3.8) is based on the no-slip boundary condition for the velocity field, and the inequality comes from the criterion $\partial\omega(P^*, T^*)/\partial t < 0$ in (3.5). Thus, we arrive at the conclusion that the vorticity field stays strictly subharmonic in a neighborhood $\boldsymbol{U}_2$ of P^*, at T^*,

$$\Delta\omega(\cdot, \cdot, T^*) < 0, \quad \text{in } \boldsymbol{U}_2; \tag{3.9}$$

like $\boldsymbol{U}_1, \boldsymbol{U}_2$ has a portion of Γ^0 as part of its boundary. Moreover, the assumption (3.4) shows that the vorticity field ω remains non-negative in $\boldsymbol{U}_1$ at the bifurcation time

$$\omega(\cdot, \cdot, T^*) \geq 0, \quad \text{in } \boldsymbol{U}_1. \tag{3.10}$$

By denoting $\boldsymbol{U}^* = \boldsymbol{U}_1 \cap \boldsymbol{U}_2$, we have, by (3.9) and (3.10),

$$\begin{cases} \Delta\omega < 0, \text{ in } \boldsymbol{U}^*, \\ \omega \geq 0, \quad \text{on } \partial\boldsymbol{U}^*. \end{cases} \tag{3.11}$$

The application of the strong maximum principle for subharmonic functions in the set $\boldsymbol{U}^*$ gives

$$\omega > 0, \quad \text{in } \boldsymbol{U}^{*0}. \tag{3.12}$$

Subsequently, the Hopf Lemma implies that

$$\frac{\partial\omega}{\partial\boldsymbol{n}}(P^*, T^*) < 0. \tag{3.13}$$

On the other hand,

$$\tau \cdot \Delta\boldsymbol{u} = \frac{\partial\omega}{\partial\boldsymbol{n}}, \quad \text{on } \Gamma^0, \tag{3.14}$$

due to the definition of vorticity $\omega = -\partial_y u + \partial_x v$ and the incompressibility condition $u_x + v_y = 0$. Consequently, taking the inner product of the momentum equation in (3.1), applied on the boundary Γ^0, with the tangential vector field τ gives

$$\frac{\partial p}{\partial\tau} = \frac{\partial p}{\partial y} = \nu\frac{\partial\omega}{\partial\boldsymbol{n}}, \quad \text{on} \quad \Gamma^0, \tag{3.15}$$

since the term $\boldsymbol{u}_t$ and the nonlinear term disappear on Γ^0 because of the no-slip boundary condition for the velocity field. The insertion of (3.13) into (3.15) results in (3.7), thus completing the proof of Theorem 3.2. □

Remark 3.3. The contribution of the pressure force to the flow acceleration for the vertical velocity field is $-\partial_y p$. We thus conclude from (3.7) that the pressure pushes the flow upward at the bifurcation point P^* when $t = T^*$, opposite to the shear flow direction. This force gives rise to the boundary-layer separation at P^* and T^* and to the recirculating flow near P^* afterward. Although the appearance of an adverse pressure gradient is well known to be the main mechanism for boundary-layer layer separation, the mathematically rigorous argument above is new and will be carefully verified in the numerical experiment presented in Section 4.

Remark 3.4. If the vorticity field stays smooth enough near the boundary segment Γ^0, then

$$\frac{\partial p}{\partial\boldsymbol{n}} = -\nu\frac{\partial\omega}{\partial\tau} = 0, \quad \text{at } (P^*, T^*); \tag{3.16}$$

the first equality in (3.16) comes from a similar argument as in (3.15), while the second one is based on the assumption that P^* is a degenerate singular point for the vorticity as stated in (3.5). Accordingly, the normal gradient of the pressure stays small near the bifurcation point, which is still consistent with the assumptions of boundary-layer theory [13,24,29]. This assertion is verified in the case of the first bifurcation time $t = T_1^*$ for the numerical example in Section 4, as can be seen in the vorticity plot along the right boundary (Fig. 6) there. At that time, the separated boundary layer is still confined to a thin layer near the wall.

The phenomenon changes dramatically at the second and later separation times. A cusp occurs in the vorticity profile at the critical point for $t = T_2^*$; see Fig. 12. The large vorticity gradient along the boundary indicates there is a strong normal pressure gradient that pushes the vortex to shed.

Remark 3.5. The critical time T^* refers to the structural bifurcation whose criteria were discussed in detail in Section 2. This is not identical to the critical time with respect to the appearance of an adverse pressure gradient. At the bifurcation point $P^* \in \partial M$ and the corresponding moment $t = T^*$, the pressure pushes the flow opposite to the basic shear flow in the immediate vicinity of P^*. In fact, the adverse pressure gradient appears at some instant $t < T^*$, and will take effect after a while, causing the recirculation. The pressure gradient can be in the same direction as the shear flow or opposite to it from time to time. The moment, however, when the pressure gradient switches sign is not the critical time that we are discussing. The rigorous derivation of the presence of an adverse pressure gradient at the bifurcation point just gives a reasonable explanation for the mechanism of boundary-layer separation.

Remark 3.6. Assumption (3.4) in Theorem 3.2, which states that pure shear flow was present near the critical point before the occurrence of the bifurcation, corresponds to the index of the vector field $\partial \boldsymbol{u}/\partial \boldsymbol{n}$ at P^* being 0, i.e., $\mathrm{ind}(\partial \boldsymbol{u}/\partial \boldsymbol{n}, P^*) = 0$.

Remark 3.7. When the shear flow is unidirectionally upward near Γ^0, rather than downward, Assumption (H) with $k = 2$ is equivalent to the following conditions:

$$\omega(P^*, T^*) = 0, \quad \frac{\partial \omega}{\partial \tau}(P^*, T^*) = 0, \qquad \frac{\partial^2 \omega}{\partial \tau^2}(P^*, T^*) < 0, \qquad \frac{\partial \omega}{\partial t}(P^*, T^*) > 0. \tag{3.17}$$

In other words, by Proposition 3.1, Assumption (H) is equivalent to either (3.5) or (3.17), depending on whether the flow is upward or downward before the critical time.

Remark 3.8. The assumption that the boundary section Γ^0 can be represented as a segment of the vertical line $x = 1$ was only made for simplicity of presentation. All the analyses in this section can be extended to the case of a horizontal or curved boundary.

Proposition 3.1 states that the criteria for the start of recirculating flow, as given in (3.5), are exactly the same as the structural bifurcation criteria stated in Section 2, i.e., a degenerate singular point for the normal derivative of the velocity vector field $\boldsymbol{u_n}$, with positive second-order derivative along the boundary and negative time derivative, appears at a boundary point $P^* \in \Gamma^0$. The proof is given below.

Proof of Proposition 3.1.

Step 1. Note that

$$\boldsymbol{v}^0 = \frac{\partial \boldsymbol{u}}{\partial \boldsymbol{n}} = \partial_x \boldsymbol{u} = (u_x, v_x) = (0, \omega), \quad \text{on } \Gamma^0. \tag{3.18}$$

The first component u_x vanishes identically because of the incompressibility condition $u_x + v_y = 0$ and the no-slip boundary condition $v \equiv 0$ on Γ^0, while the second component v_x is exactly the vorticity field since

$$\omega = -u_y + v_x = v_x, \quad \text{on } \Gamma^0, \tag{3.19}$$

due to the no-penetration boundary condition $u \equiv 0$ on Γ^0. According to (3.18), the singular point for $\boldsymbol{v}^0$ is the same as the zero point for ω on the boundary section Γ^0. As a result, the Prandtl condition (2.2) in Assumption (H) is equivalent to the first condition in (3.6), i.e., the vanishing of the vorticity ω at (P^*, T^*).

Step 2. Furthermore, the vorticity field has the same tangential derivatives as v_x to any order, i.e., for any integer $k = 1, 2, 3, \ldots$,

$$\partial_\tau^k \omega = \partial_\tau^k(-u_y + v_x) = -\partial_y^k u_y + \partial_y^k v_x = -\partial_y^{k+1} u + \partial_y^k v_x = \partial_\tau^k v_x, \quad \text{on } \Gamma^0, \tag{3.20}$$

due to the the no-penetration boundary condition for u. Note that the term v_x is exactly the tangential component of the normal derivative of the velocity field, i.e., $v_x = \boldsymbol{v}_\tau^0$. Thus, the third condition in (3.6), $\partial^2 \omega(P^*, T^*)/\partial^2 \tau \neq 0$, is equivalent to the technical condition (2.5) in Assumption (H) with $k = 2$.

Step 3. The necessary condition (2.3) in Assumption (H) is exactly equivalent to the condition that the Jacobian matrix D of $\boldsymbol{u_n}$ at the critical point $(\boldsymbol{x}_0, t_0)$ is degenerate, i.e.,

$$\det\left(D\frac{\partial \boldsymbol{u}}{\partial \boldsymbol{n}}\right) = \det\begin{pmatrix} u_{xx} & u_{xy} \\ v_{xx} & v_{xy} \end{pmatrix} = 0, \quad \text{at } \boldsymbol{x}_0 \in \Gamma^0. \tag{3.21}$$

On the other hand, u_{xy} is identically zero on Γ^0 since u_x is, as shown in (3.18). Hence, (3.21) is the same as

$$\det\left(D\frac{\partial \boldsymbol{u}}{\partial \boldsymbol{n}}\right) = \det\begin{pmatrix} u_{xx} & u_{xy} \\ v_{xx} & v_{xy} \end{pmatrix} = u_{xx}v_{xy} = -(v_{xy})^2 = 0, \quad \text{at } \boldsymbol{x}_0 \in \Gamma^0; \tag{3.22}$$

the last step in (3.22) is based on the identity that $u_{xx} \equiv -v_{xy}$, due to the incompressibility of $\boldsymbol{u} = (u, v)$. The only possible solution for (3.22) is given by $v_{xy} = 0$, which implies that

$$\partial_\tau \omega = \omega_y = -u_{yy} + v_{xy} = v_{xy} = 0, \quad \text{at } \boldsymbol{x}_0 \in \Gamma^0. \tag{3.23}$$

Therefore, we proved that the necessary condition (2.3), $\mathrm{ind}(\boldsymbol{v}^0, \boldsymbol{x}_0) \neq -1/2$ in Assumption (H), is equivalent to the second condition in (3.6).

Step 4. Next we show the equivalence between the second necessary condition (2.4), $\boldsymbol{v}^1(\boldsymbol{x}_0) \neq 0$ in Assumption (H), and the fourth condition in (3.6), $\partial\omega(P^*, T^*)/\partial t \neq 0$. We recall from the Taylor expansion (2.1) that $\boldsymbol{v}^1 = \partial_t \boldsymbol{v}^0$. The insertion of the evaluation (3.18) gives

$$\boldsymbol{v}^1 = \partial_t(0, \omega) = (0, \frac{\partial \omega}{\partial t}), \quad \text{on } \Gamma^0, \tag{3.24}$$

which leads to the equivalence between (2.4) and the last condition in (3.6).

The first part of Proposition 3.1 is thus proven. The verification of the second part is essentially the same and we omit the details here. □

4. Numerical example of driven-cavity flow

In this section, we give a numerical verification of the necessary and sufficient criteria for structural bifurcation in 2-D incompressible flow by presenting an example of smoothly started, driven-cavity flow at Reynolds number $Re = 10^5$.

4.1. Formulation of the problem

We consider the flow in a nondimensional square cavity $M = [0, 1] \times [0, 1]$, which is driven by slip velocity with a parabolic profile on the top boundary. The flow is governed by the 2-D incompressible Navier–Stokes equations (3.1). The boundary ∂M in (3.2) is now composed of four sections: the left, right and bottom boundary sections are denoted by Γ_r and the top section is denoted by Γ_t. The following Dirichlet boundary conditions for the velocity field are imposed

$$\begin{aligned} &\boldsymbol{u} = 0, \quad \text{on } \Gamma_\mathrm{r}, \\ &u = u_s = 16x^2(1-x)^2, \quad v = 0, \text{ on } \Gamma_\mathrm{t}; \end{aligned} \tag{4.1}$$

u_s denotes the slip velocity along the top boundary that drives the flow inside the cavity. In other words, no-slip boundary conditions are imposed on Γ_r and a purely tangential velocity is prescribed on the top boundary Γ_t.

The initial velocity profile is taken as

$$u(x, y, 0) = -16x^2(1-x)^2(2y-3y^2), \quad v(x, y, 0) = 32(x-3x^2+2x^3)(y^2-y^3), \tag{4.2}$$

so that the flow is started smoothly.

4.1.1. Vorticity formulation

Equations (3.1) can be written in the vorticity–stream function formulation

$$\begin{cases} \partial_t \omega + (\boldsymbol{u}\cdot\nabla)\omega = \nu\Delta\omega, \\ \Delta\psi = \omega, \\ u = -\partial_y\psi, \quad v = \partial_x\psi, \end{cases} \tag{4.3}$$

where ω is the vorticity, as in (3.3), and ψ the stream function. The boundary conditions for velocity can be expressed as boundary conditions for the stream function. The no-penetration boundary condition $\boldsymbol{u}\cdot\boldsymbol{n} = 0$ is equivalent to $\partial\psi/\partial\tau\,|_{\Gamma} = 0$ and thus, without loss of generality, to the homogeneous Dirichlet boundary condition $\psi\,|_{\Gamma} = 0$. The no-slip boundary condition $\boldsymbol{u}\cdot\tau = 0$, which is imposed on Γ_r, is equivalent to a Neumann boundary condition for the stream function $\partial\psi/\partial\mathbf{n}\,|_{\Gamma_r} = 0$, while the boundary condition on the top boundary Γ_t can be written as $\partial\psi/\partial y\,|_{\Gamma_t} = -u_s = -16x^2(1-x)^2$. We thus have the following boundary conditions for the stream function:

$$\begin{aligned} &\psi = 0, \qquad \text{on } \partial M, \\ &\tfrac{\partial\psi}{\partial\mathbf{n}}\,|_{\Gamma_r} = 0, \ \tfrac{\partial\psi}{\partial y}\,|_{\Gamma_t} = -u_s = -16x^2(1-x)^2. \end{aligned} \tag{4.4}$$

4.2. Numerical method

The closed system (4.3), (4.4) is solved using the EC4 scheme developed by E and Liu [8] and analyzed by C. Wang and J.-G. Liu [31,32]. A regular grid $\{x_i = i/N, y_j = j/N, i, j = 0, 1, \ldots, N\}$, with mesh size $\Delta x = \Delta y = h = 1/N$ is used to cover the computational domain M. Let $\tilde{D}_x$ and $\tilde{D}_y$ represent the standard second-order centered-difference approximation to ∂_x and ∂_y, D_x^2 and D_y^2 be second-order centered-difference approximations to ∂_x^2 and ∂_y^2, and $\Delta_h = D_x^2 + D_y^2$ the standard five-point Laplacian. The term "compact" in the name of the EC4 scheme refers to the stencil needed to evaluate the derivatives being as small as possible.

4.2.1. Description of EC4 scheme

The starting point of the scheme is the fact that the Laplacian operator Δ can be estimated with fourth-order accuracy by

$$\Delta_4 = \frac{\Delta_h + (h^2/6)D_x^2 D_y^2}{1 + (h^2/12)\Delta_h} + \mathrm{O}(h^4). \tag{4.5}$$

Multiplying the momentum equation by the difference operator $1 + (h^2/12)\Delta_h$ gives

$$(1 + \tfrac{1}{12}h^2\Delta_h)\partial_t\omega + (1 + \tfrac{1}{12}h^2\Delta_h)\nabla\cdot(\boldsymbol{u}\omega) = \nu(\Delta_h + \tfrac{1}{6}h^2 D_x^2 D_y^2)\omega, \tag{4.6}$$

while the same operation applied to the kinematic equation $\Delta\psi = \omega$ results in

$$(\Delta_h + \tfrac{1}{6}h^2 D_x^2 D_y^2)\psi = (1 + \tfrac{1}{12}h^2\Delta_h)\omega. \tag{4.7}$$

The homogeneous Dirichlet boundary condition $\psi\,|_{\Gamma} = 0$ can be used to solve the discrete Poisson-like equation (4.7) very efficiently, using a sine transform. The Neumann boundary condition for the stream function can be converted into a boundary condition for the vorticity in solving (4.6); it will be given in detail later.

The nonlinear convection term in (4.6) is estimated as

$$(1+\tfrac{1}{12}h^2\Delta_h)(\boldsymbol{u}\cdot\nabla\omega) = \tilde{D}_x(1+\tfrac{1}{6}h^2D_y^2)(u\omega) + \tilde{D}_y(1+\tfrac{1}{6}h^2D_x^2)(v\omega) - \tfrac{1}{12}h^2\Delta_h(u\tilde{D}_x\omega + v\tilde{D}_y\omega) + \mathrm{O}(h^4). \tag{4.8}$$

The first two terms on the right-hand side of (4.8) are compact. Although the third term is not compact, it does not cause any trouble in practical computation: $u\tilde{D}_x\omega + v\tilde{D}_y\omega$ can be taken as 0 on Γ_r because of the no-slip boundary condition, and the corresponding term on the top boundary Γ_t can be treated in a similar fashion as

$$(u\tilde{D}_x\omega + v\tilde{D}_y\omega)_{i,N} = u_\mathrm{s}\cdot(\tilde{D}_x\omega)_{i,N}, \tag{4.9}$$

where u_s is the slip velocity on Γ_t, as given in (4.1).

By introducing an intermediate variable $\bar{\omega}$

$$\bar{\omega} = (1+\tfrac{1}{12}h^2\Delta_h)\omega, \tag{4.10}$$

and combining (4.6)–(4.10), the whole momentum equation can be approximated by

$$\partial_\mathrm{t}\bar{\omega} + \tilde{D}_x(1+\tfrac{1}{6}h^2D_y^2)(u\omega) + \tilde{D}_y(1+\tfrac{1}{6}h^2D_x^2)(v\omega) - \tfrac{1}{12}h^2\Delta_h(u\tilde{D}_x\omega + v\tilde{D}_y\omega) = \nu(\Delta_h + \tfrac{1}{6}h^2D_x^2D_y^2)\omega. \tag{4.11}$$

The velocity $\boldsymbol{u} = \nabla^\mathrm{T}\psi = (-\partial_y\psi, \partial_x\psi)$ can be obtained by the fourth-order approximation to ∂_x and ∂_y

$$u = -\tilde{D}_y(1-\tfrac{1}{6}h^2D_y^2)\psi, \qquad v = \tilde{D}_x(1-\tfrac{1}{6}h^2D_x^2)\psi, \tag{4.12}$$

which is not compact.

The vorticity ω is determined from $\bar{\omega}$ via (4.10). To solve the Poisson-like equation (4.10) requires a boundary condition for ω, which is discussed in the following subsection.

4.2.2. Boundary condition for vorticity

The boundary values for the vorticity are very important in order to capture the exact location of its singular point, as well as the critical moment T^* and the bifurcation point P^* of Section 3, and thus help illustrate the detailed process of vortex shedding. Physically the vorticity boundary condition enforces the no-slip boundary condition for the velocity. More precisely, one converts the Neumann boundary condition for the stream function into $\omega\,|_\Gamma$ by the kinematic relation $\Delta\psi = \omega$. On the right boundary section where $x = 1$, $i = N$, either Briley's formula [2,8]

$$\omega_{N,j} = \frac{1}{18h^2}(108\psi_{N-1,j} - 27\psi_{N-2,j} + 4\psi_{N-3,j}), \tag{4.13}$$

or a new fourth-order formula for the vorticity [32],

$$\omega_{N,j} = \frac{1}{h^2}\left(8\psi_{N-1,j} - 3\psi_{N-2,j} + \tfrac{8}{9}\psi_{N-3,j} - \tfrac{1}{8}\psi_{N-4,j}\right), \tag{4.14}$$

can be applied to solve (4.10).

Both Briley's formula (4.13) and the new formula (4.14) are derived by combining the Dirichlet boundary condition $\psi\,|_{x=1} = 0$ and the Neumann boundary condition $\partial\psi/\partial x\,|_{x=1} = 0$ for the stream function. It was proven in [31,32] that the above one-sided vorticity boundary conditions are consistent with the centered differences applied at interior points. In addition, both formulas preserve stability and result in fourth-order accuracy for the 2-D Navier–Stokes equations. For computational convenience, we use Briley's formula in the calculation. On the top boundary,

where the slip velocity u_s given in (4.1) drives the flow in the cavity, the corresponding Briley's formula turns out to be [2,31,32]:

$$\omega_{i,N} = \frac{1}{18h^2}(108\psi_{i,N-1} - 27\psi_{i,N-2} + 4\psi_{i,N-3}) - \frac{11}{3h}u_s(x_i). \tag{4.15}$$

The stability analysis of the final scheme and the relevant convergence theorems guarantee the accuracy of the profiles reported in this section.

4.2.3. Temporal discretization

To solve the time-dependent system of spatially discretized equations obtained by the above finite-difference method, we use a fourth-order Runge–Kutta method in time. It was argued in [7] that the stability concern associated with the cell Reynolds number constraint can be avoided in higher-order Runge-Kutta methods. One advantage of the EC4 scheme is that at each time step or, more precisely, at each stage in Runge-Kutta time stepping, only two Poisson solvers, (4.7) and (4.10), are required to achieve fourth-order accuracy. In addition, the vorticity boundary condition is explicitly enforced.

The combination of these features makes the whole scheme quite efficient, accurate and robust. All the figures in Section 4.3 below are plotted at $N = 1536$, where the numerical results have clearly stabilized.

4.3. Structural bifurcation

The velocity u_s along Γ_t drives the flow clockwise in the cavity. We call this clockwise rotation the basic circulation. As a result of this circulation, the flow moves downward near the mid-portion of the right boundary. We concentrate on this area, which is away from the corners, to illustrate the flow's behavior with respect to the issue of structural bifurcation caused by boundary-layer separation. In other words, the recirculation areas near the corners are not taken into consideration, since they are caused by corner singularity rather than by boundary-layer separation. The contour plot of the stream function at time $t = 1$ in Fig. 2 shows the structure of the basic circulation.

Near the mid-portion of the right boundary, the tangential velocity v is negative, as a result of the basic circulation. The combination of the no-slip boundary condition and the basic circulation results in the presence of a thin boundary layer, due to the sharp, initially monotone transition of the velocity from zero tangential velocity on the boundary to a negative value of v in the interior. The width of this layer is proportional to $O(Re^{-1/2})$ [13,24]. Accordingly, the vorticity $\omega = -\partial_y u + \partial_x v$ is positive in the boundary layer, at least initially. The vorticity near and on the right boundary at $t = 1$ is plotted in Fig. 3.

As shown in Fig. 3(b), the vorticity has positive values along much of the right boundary, say, from 0.5 to 0.9 in y. The negative vorticity along the top and bottom portions comes from the recirculation in the two corner areas, which is not considered here. The two singular points for the vorticity on the right boundary, at $y_1 = 0.4365$, $y_2 = 0.9531$, are non-degenerate, i.e, the tangential derivative $\partial\omega/\partial y$ is nonzero. Thus the criterion given in Section 2 indicates that the flow structure stays stable for the moment and no transition in the flow's topological structure is going to occur. Moreover, the zoom plot in Fig. 3(a) tells us that the whole vorticity field remains positive near the mid-portion of the right boundary at $t = 1$. Thus, only shear flow is present in the boundary layer before the separation, in this region.

Classical boundary-layer theory is covered in [4,13,24,29]. Aside from the references already given at the beginning of Section 1, the mathematical analysis of the Prandtl equation is reviewed in [5]. Global weak solutions for the Prandtl equation were shown to exist by Zhang and Xin in [35]. The blow-up of the Prandtl equation, as established by E and Engquist in [6], bears no relationship to boundary-layer separation, as far as we can tell, since the assumptions under which the Prandtl equation is derived cease to be valid when separation occurs. A detailed numerical study of the zero-viscosity limit for the flow past a cylinder, including boundary-layer separation, appears in [15].

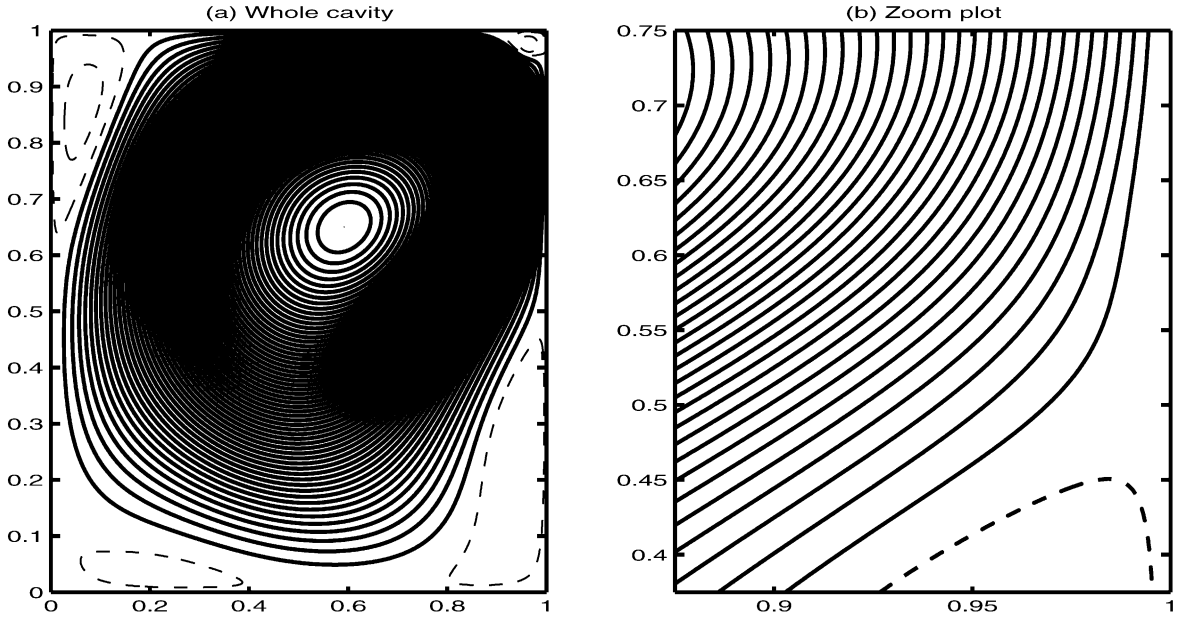

Fig. 2. Contour plot of the stream function at time $t = 1$: (a) over the whole square cavity $[0, 1]^2$; (b) zoom plot in the region $[7/8, 1] \times [3/8, 3/4]$ near the mid-portion of the right boundary.

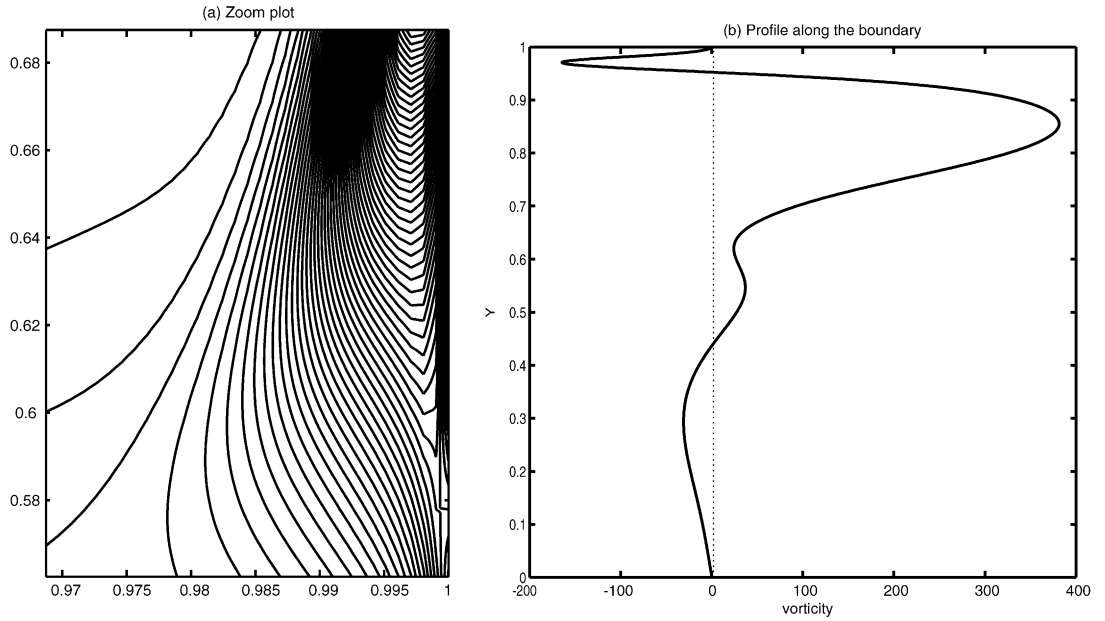

Fig. 3. Vorticity plot at time $t = 1$: (a) zoomed contour plot in the region $[31/32, 1] \times [9/16, 11/16]$; (b) vorticity profile along the right boundary $x = 1$.

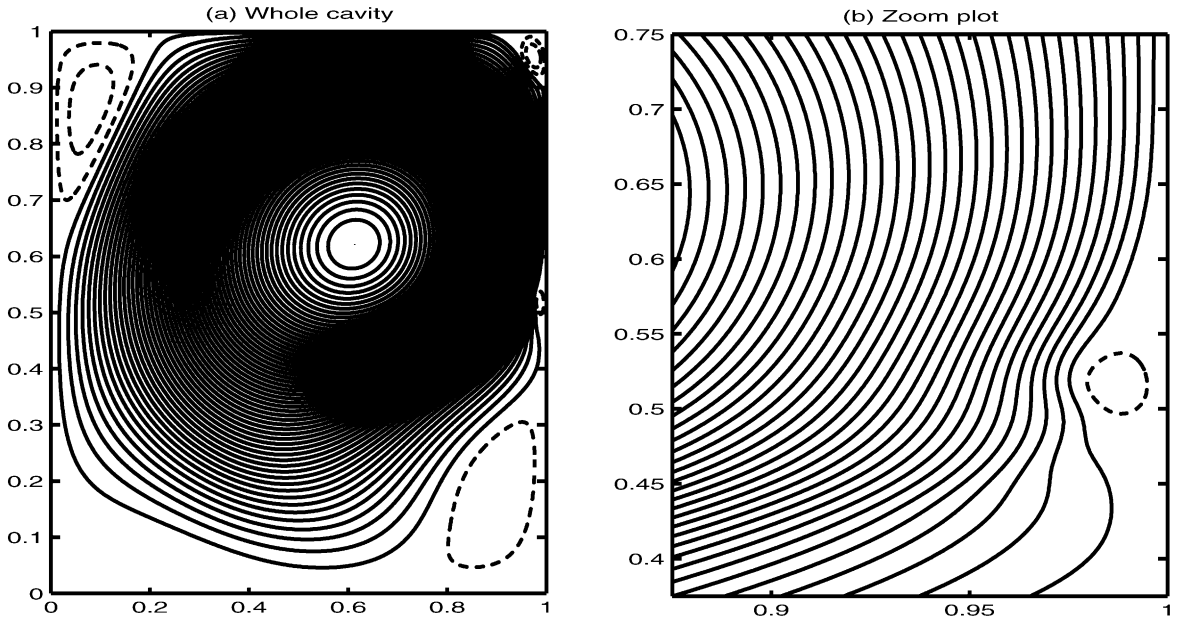

Fig. 4. Stream function plot at time $t = 1.5$: (a) over the whole square cavity; and (b) zoom plot in the same region as in Fig. 2(b).

As mentioned before, the main objective in this article is to study the structural transition of the flow in the boundary layer, analytically and numerically. The structural transition criteria discussed in Section 2 do apply to the right boundary, since a no-slip boundary condition is imposed there. Our numerical simulation shows that the vorticity along the mid-portion of the right boundary remains positive for quite a while after the initial time $t = 0$. During this time interval, the boundary-layer structure is regular and its regularity persists until boundary-layer separation occurs. This numerical evidence suggests that boundary-layer separation occurs before the blow-up predicted in [6].

4.3.1. The first structural bifurcation

At time $t = 1.5$, Fig. 4 presents stream function plots and Fig. 5 shows the vorticity field near the right boundary, and its profile along the boundary. The differences in the flow structure between $t = 1$ and $t = 1.5$ can be clearly seen by comparing Figs. 2 and 3, on the one hand, and Figs. 4 and 5, on the other.

At $t = 1$, Fig. 2(b) shows that there is no recirculation near the mid-portion of the right boundary. Accordingly, Fig. 3(b) indicates that the vorticity profile along the right boundary is positive in the mid portion: no degenerate singular point for the vorticity forms and the flow structure is stable at this time. At time $t = 1.5$, recirculation is obviously apparent in the zoom contour plot of Fig. 4(b). Fig. 5(b) shows that there are two nondegenerate singular points for vorticity ($Y_1^0 = 0.4590$, $Y_2^0 = 0.5370$) on the right boundary near its middle. Moreover, a 2-D area with negative vorticity is illustrated in Fig. 5(a), whose boundary is composed of the boundary section between $(1, Y_1^0)$ and $(1, Y_2^0)$ on Γ_r and a smooth curve inside the interior of the cavity that connects the two singular points.

We conclude that a structural transition occurs between $t = 1$ and $t = 1.5$. Detailed inspection of the numerical results shows that the first singular point for vorticity on the right boundary appears at $T_1^* = 1.0788$ and $Y_1^* = 0.6107$. The vorticity profile along the boundary at that moment is plotted in Fig. 6(a), where the degenerate singular point appears at $y = Y_1^*$; the time history of the vorticity at the boundary point $(1, Y_1^*)$ is given in Fig. 6(b).

By Theorem 2.8, the velocity vector field is structurally unstable at that moment. It is clear from Fig. 6 that the vorticity reaches zero at $(1, Y_1^*; T_1^*)$ as a local minimum in space and decreases in time, i.e, $\omega(1, Y_1^*; T_1^*) = 0$,

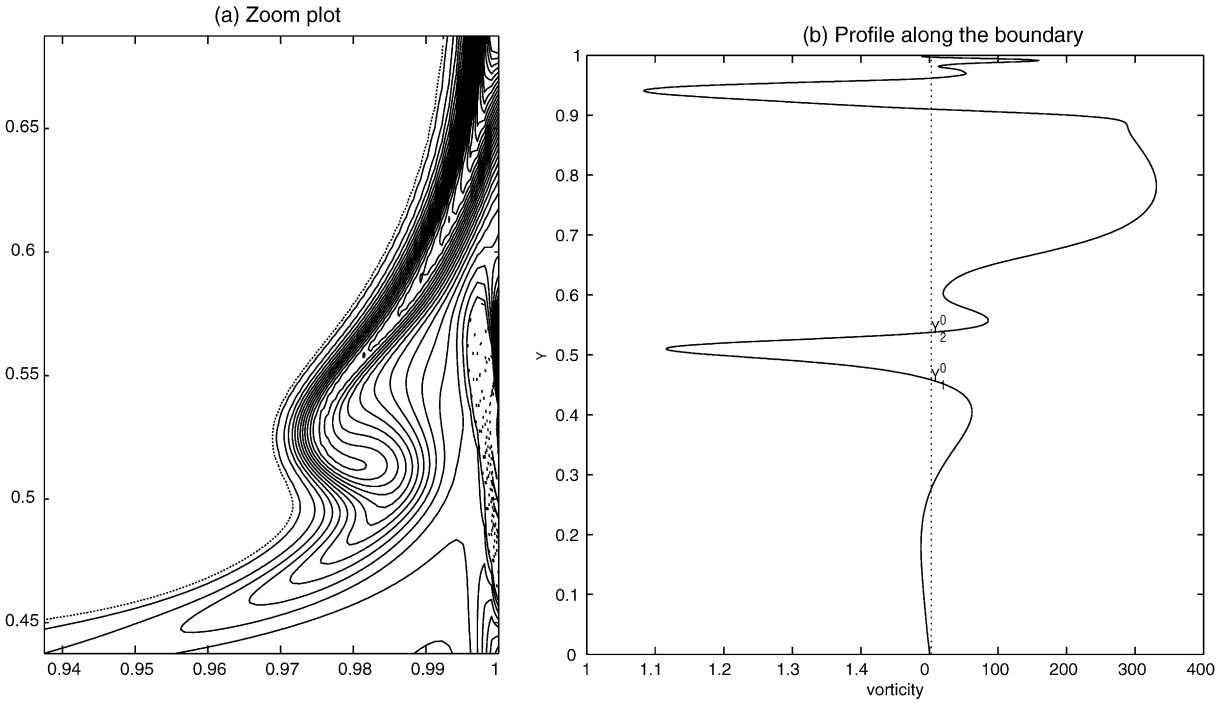

Fig. 5. Vorticity plot at time $t = 1.5$. (a) Zoomed contour plot in the region $[15/16, 1] \times [7/16, 11/16]$; the solid and dotted lines represent the contours for the positive and negative levels, respectively. (b) Vorticity profile along the right boundary.

$\partial\omega(1, Y_1^*; T_1^*)/\partial y = 0$, $\partial^2\omega(1, Y_1^*; T_1^*)/\partial^2 y > 0$, $\partial\omega(1, Y_1^*; T_1^*)/\partial t < 0$, so that the condition (3.5) is satisfied. This condition is equivalent to Assumption (H) for structural transition, by Proposition 3.1, given $k = 2$ in the technical condition (2.5). The detailed bifurcation process is outlined in the proof of Theorem 2.8, with respect to the local structure of the velocity field in a neighborhood which contains the boundary point $P_1^* = (1, Y_1^*)$ [11]; see also Fig. 1 here.

When $t < T_1^*$, there is no singular point for vorticity in the mid-portion of the right boundary, and the local structure of the stream function near that boundary section is equivalent to Fig. 1(a), as seen in Fig. 2(b) at $t = 1$.

When $t = T_1^*$, there is one degenerate singular point for vorticity, which is a local minimum on Γ_r and decreases in time, as shown in Fig. 6(a) and (b). The local structure of the stream function near the mid-portion of the right boundary is now equivalent to Fig. 1(b).

When $t > T_1^*$, there are two isolated singular points for vorticity on Γ_r, and their orbits are connected. For example, at $t = 1.5$, it appears in Fig. 5(b) that the locations of the two isolated singular points are $Y_1^0 = 0.4590$, $Y_2^0 = 0.537$. The zoom plot in Fig. 4(b) shows that the local structure of the stream function near those two points is equivalent to Fig. 1(c). The zoom plot of the tangential velocity v in Fig. 7 shows that the near-boundary flow is really reversed between Y_1^0 and Y_2^0.

Theorems 2.8 and 3.2 assure the occurrence of structural transition of the flow at the time $t = T_1^*$. The phenomenon of boundary-layer separation is a physical explanation of such bifurcation in the case of 2-D viscous incompressible flows. Furthermore, it is shown in Fig. 8 that ω stays positive in a small 2-D neighborhood of the bifurcation point $(1, Y_1^*)$ and it has a negative normal derivative at that point. Consequently, the pressure pushes the flow upward, i.e, opposite to the direction of the basic circulation. This numerical result matches our argument in Section 3 and the effects on the flow at a somewhat later time can also be seen in the velocity plot of Fig. 7.

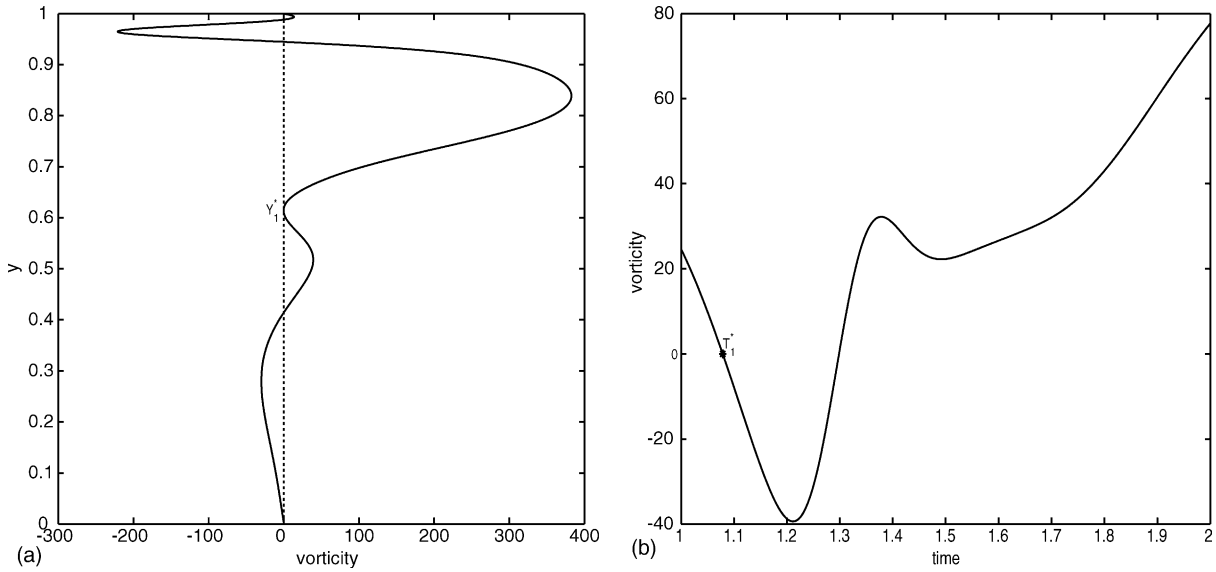

Fig. 6. Vorticity behavior on the boundary. (a) The vorticity profile along the boundary at $t = T_1^* = 1.0788$; and (b) the evolution of the vorticity at the first bifurcation point $P_1^* = (1, Y_1^*)$, $Y_1^* = 0.6107$.

In addition, we conclude from the equality (3.16) in Remark 3.2 that the normal derivative of the pressure vanishes at the first bifurcation point $(1, Y_1^*)$ and the first bifurcation time $t = T_1^*$; indeed, the vorticity field stays sufficiently smooth near the right boundary, as seen in Figs. 6(a) and 7(a). As a result, the normal gradient of the pressure remains small near the bifurcation point $(1, Y_1^*)$, and thus, for some time after the first bifurcation, the main effect

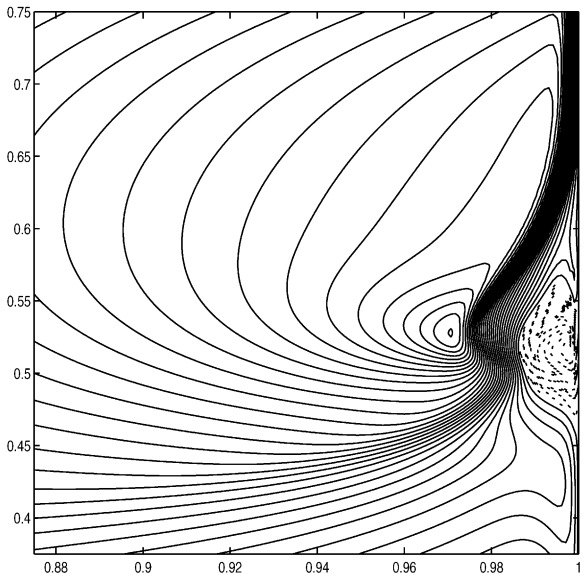

Fig. 7. Zoom plot of the vertical velocity near the right boundary at $t = 1.5$. Solid lines for downward velocity, dotted lines for upward velocity.

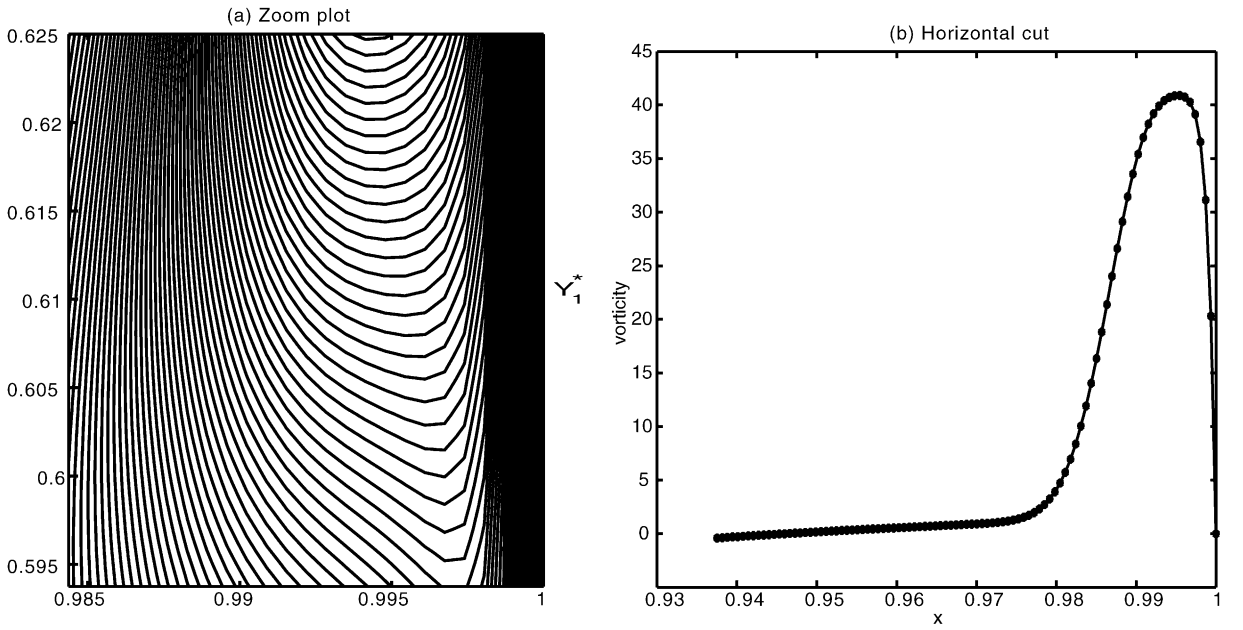

Fig. 8. Vorticity plot at the first critical time $t = T_1^*$. (a) Zoom plot in the region $[63/64, 1] \times [19/32, 5/8]$; same convention as in Fig. 5(a). (b) Vorticity profile along the horizontal cut $y = Y_1^* = 0.6107$ near the first bifurcation point.

of the pressure force nearby is to accelerate the fluid in the direction opposite to the basic circulation. For a certain time, the boundary layer is still confined to a thin layer near the wall.

4.3.2. Second bifurcation

As time goes on, the recirculation vortex expands and moves downward along the right boundary, i.e., in the same direction as the basic circulation. This can be seen in Fig. 9, which gives the stream function field at $t = 1.75$.

As this first recirculation vortex is swept along the wall by the basic circulation, the process of flow reversal near the wall, as described in Section 4.3.1, is repeated, including the details of the transition in the flow pattern. Fig. 10 presents the stream function plots when $t = 2$, after the second bifurcation time.

The difference in flow structure between $t = 1.75$ and $t = 2$ can be verified by the evolution of the vorticity profile along the right boundary, plotted in Fig. 11. Our numerical results indicate that the second critical time is $T_2^* = 1.8086$, and the position of the singular point for the vorticity at that time is $Y_2^* = 0.5182$; see Fig. 12.

Similar to the first bifurcation, the zoom plot for the vorticity near the second bifurcation point at $t = T_2^*$, as presented in Fig. 13(a), shows that the vorticity field stays positive in a small 2-D neighborhood of the structural bifurcation point $P_2^* = (1, Y_2^*)$. In fact, the shear flow structure is still preserved in a narrow strip at that moment. A narrow upward jet runs parallel to the right wall but stays in the interior, away from the boundary layer at the critical moment. Consequently, a negative normal derivative for the vorticity at the point P_2^* can be seen in Fig. 13(b). This validates, once more, the upward push of the pressure near a structural bifurcation point.

As pointed out in Remark 3.2, the first equality in (3.16) states that there is no normal pressure force at the bifurcation point. This statement is true for the first bifurcation time, but not the second bifurcation time. The vorticity profile has a cusp at the critical point $(1, Y_2^*)$, rather than a smooth minimum; see Fig. 12(a). In addition, the tangential derivative of the vorticity along the right wall, $x = 1$, changes sign across $y = Y_2^*$; this indicates

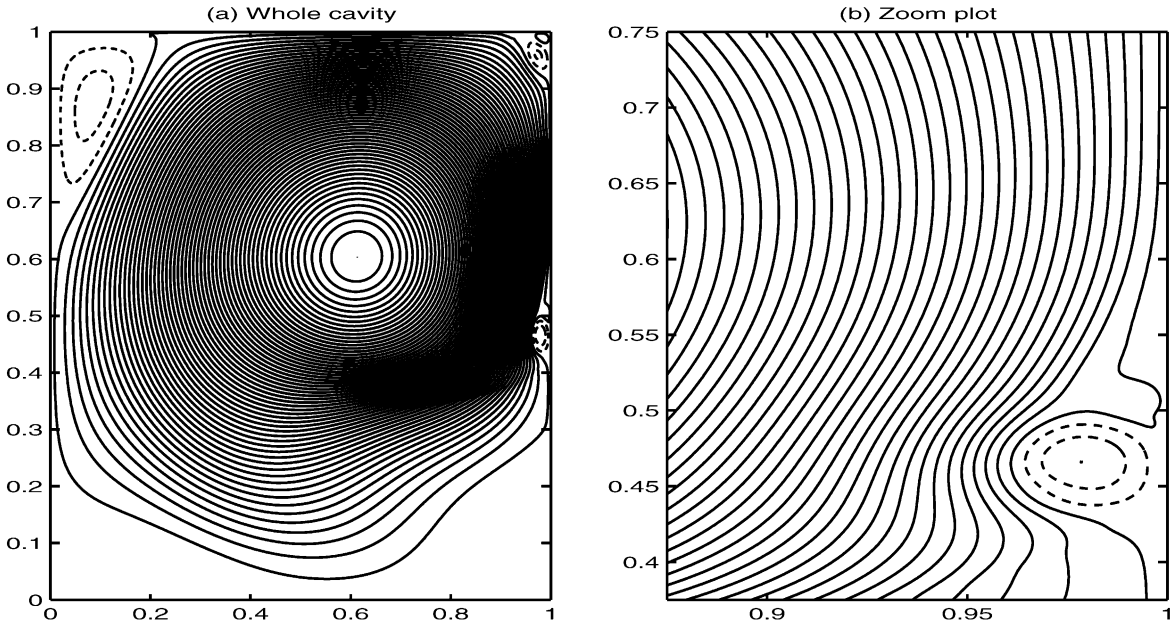

Fig. 9. Stream function plot at time $t = 1.75$: (a) over the whole cavity; (b) zoom in the region $[7/8, 1] \times [3/8, 3/4]$.

that a pair of vortices with opposite signs forms at the same time. Such a vortex pair formation is common during boundary-layer separation. Another peak in the vorticity profile along the wall appears near the critical point, as shown in Fig. 12(a). The large tangential derivative of the vorticity along the boundary is associated with a strong normal pressure gradient, which pushes the vortex formed at $t = T_1^*$ to shed.

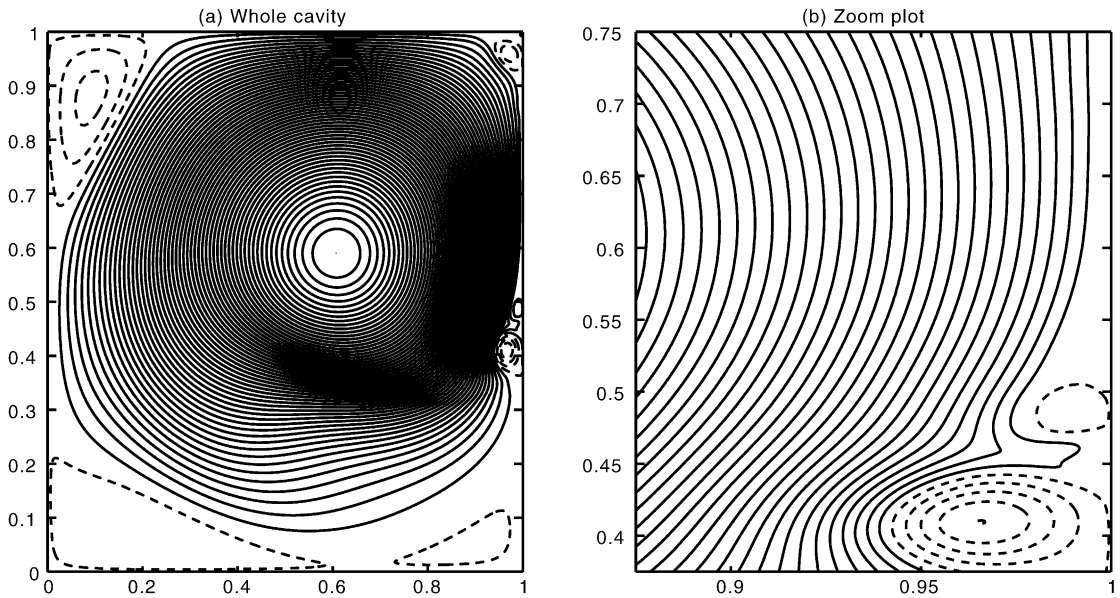

Fig. 10. Stream function plot at time $t = 2$: (a) over the whole cavity; (b) zoom in the same region as in Fig. 9(b).

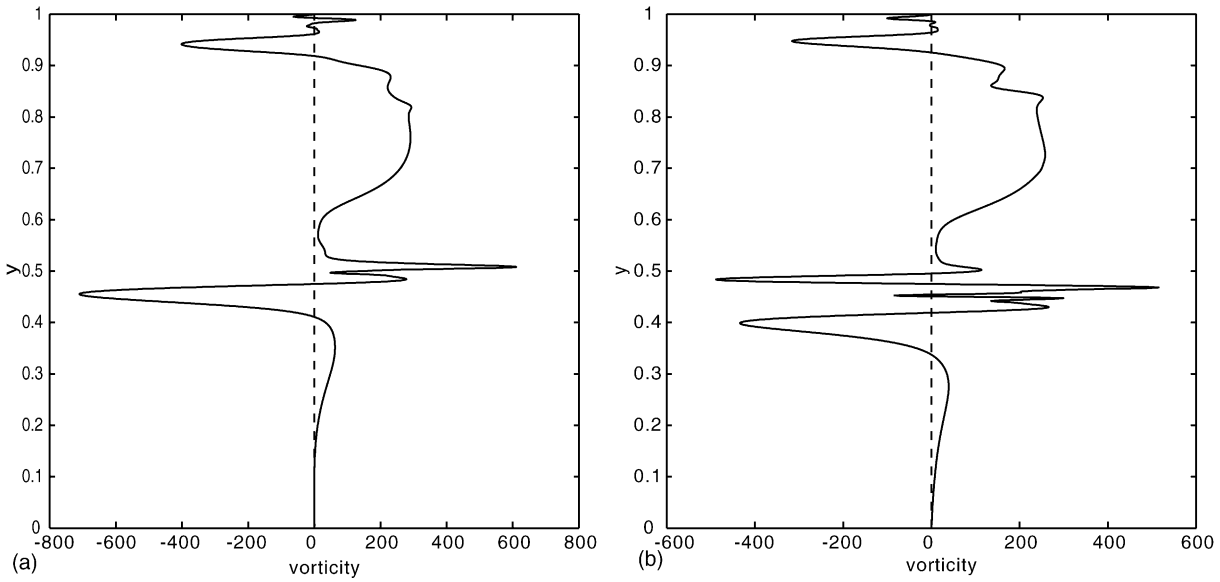

Fig. 11. Vorticity profile along the right wall: (a) $t = 1.75$; and (b) $t = 2$.

The second bifurcation time appears thus to be a crucial moment for boundary-layer separation of incompressible flow, as it marks the critical moment for the onset of vortex shedding. After this moment, the vorticity starts to roll up, as can be clearly seen in Fig. 14(a)–(c).

Meanwhile, the "first" vortex detached from the wall moves deeper into the cavity, due to the interaction between the boundary layer and the flow in the interior. From this point on, the evolution of the first detached eddy depends more and more on its interaction with the interior flow.

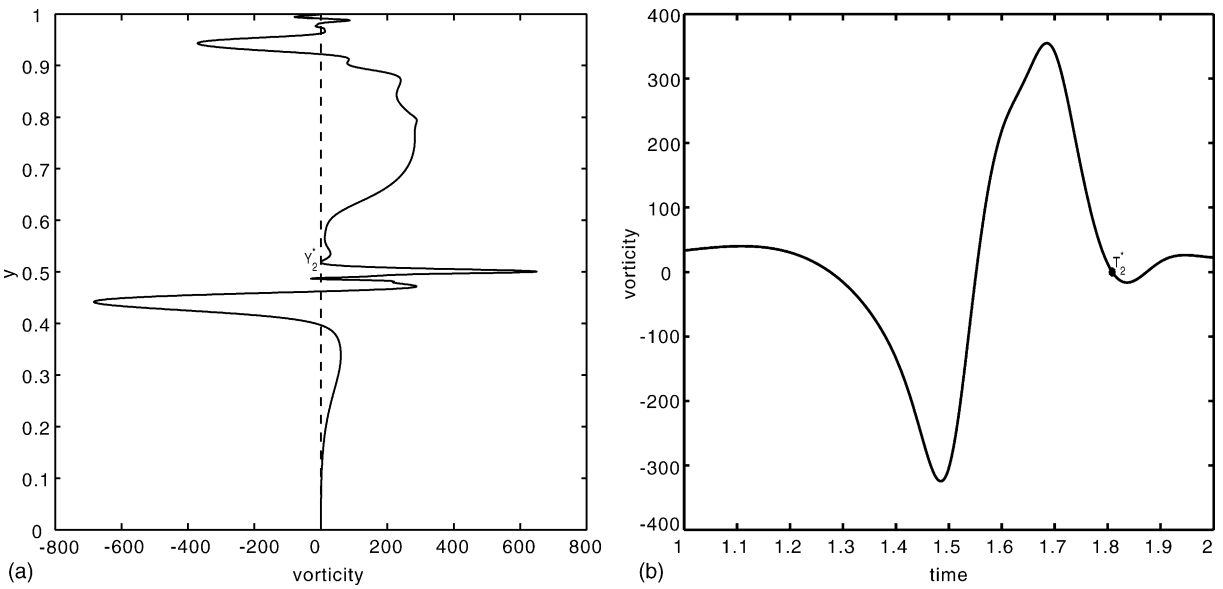

Fig. 12. Vorticity behavior on the boundary: (a) vorticity profile along the boundary at the second critical time $t = T_2^* = 1.8086$; and (b) the evolution of the vorticity at the second bifurcation point $P_2^* = (1, Y_2^*)$, $Y_2^* = 0.5182$.

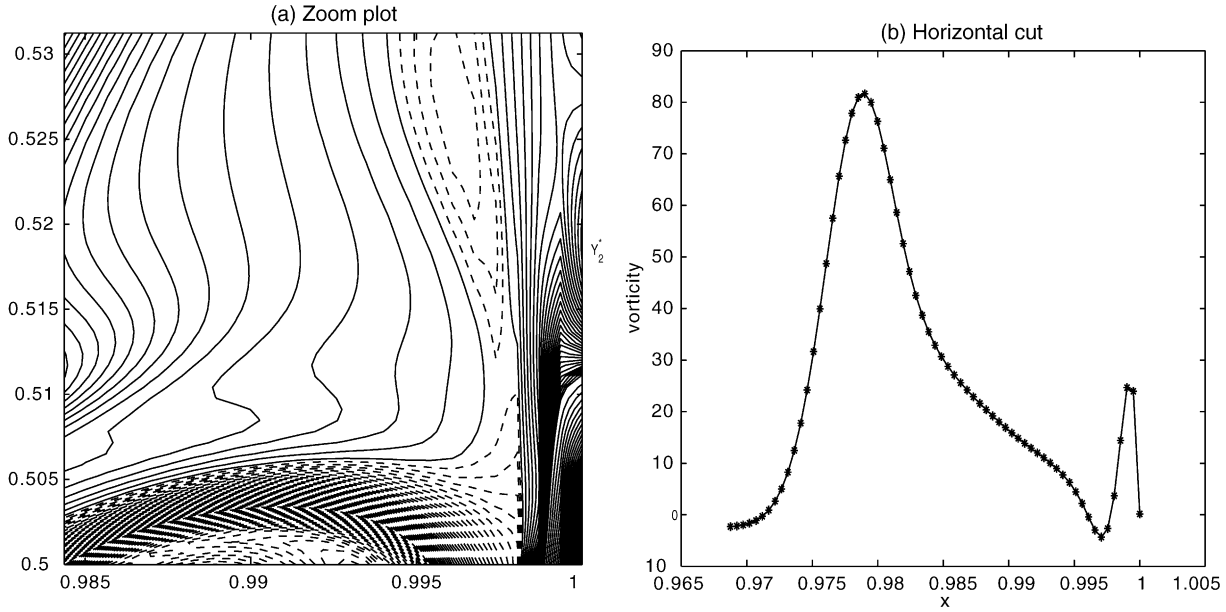

Fig. 13. Vorticity plot at the second critical time $t = T_2^*$: (a) zoom plot in the region $[63/64, 1] \times [1/2, 17/32]$; and (b) vorticity along the horizontal cut $y = Y_2^* = 0.5182$.

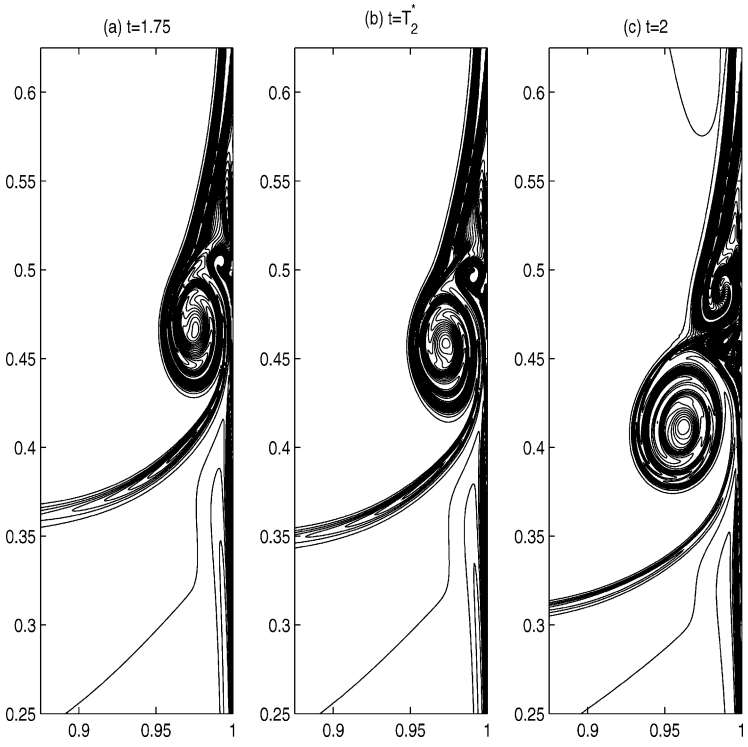

Fig. 14. Zoom plots of vorticity near the right wall at: (a) $t = 1.75$; (b) $t = T_2^* = 1.8086$; and (c) $t = 2$.

4.3.3. Multiple eddies and interactions with the interior flow

Throughout the time history of the vorticity profile along the right boundary, degenerate singular points appear again and again. Thus more and more vortices form along the boundary, detach from it, and move into the interior afterward. The process of structural transition and formation of a recirculation zone each time is the same.

Another interesting phenomenon is the structural bifurcation caused by an eddy that moves into the interior region. By the singularity classification theory for interior points (see [10,19], recapitulated here as Theorem 2.6), a bifurcation in the interior is likely to happen if a degenerate singular point of the velocity vector field appears there. This issue will be addressed in detail in a future article. A sequence of such topological transitions is illustrated in the sequence of zoom plots of the stream function near the right wall at the later times $t = 2$, 2.375, 2.75, 3, 3.5, and 4 in Fig. 15(a)–(f).

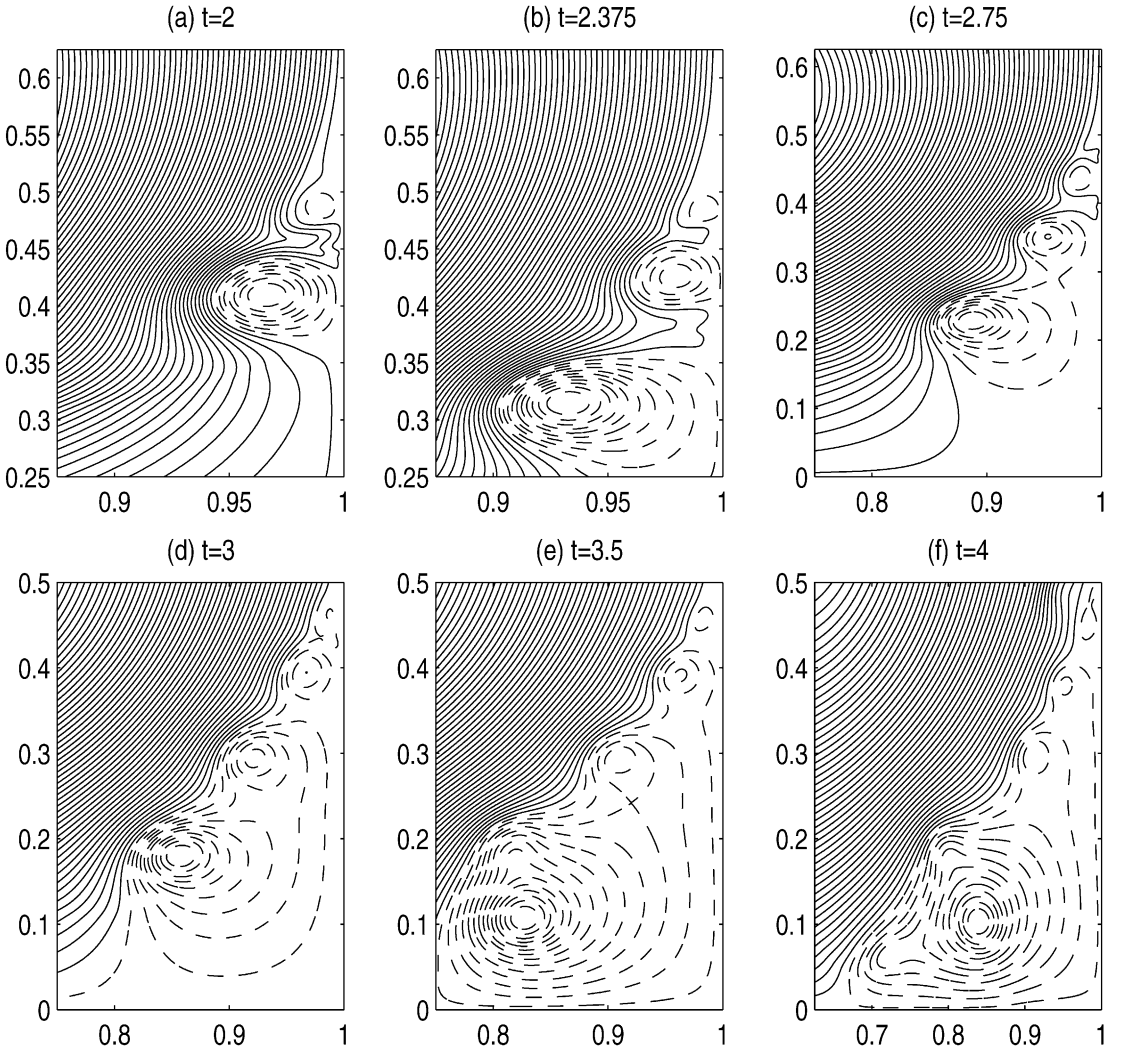

Fig. 15. Zoom plots of the stream function field near the right wall of the cavity at a sequence of times after the second bifurcation: (a) $t = 2.0$; (b) 2.375; (c) 2.75; (d) 3.0; (e) 3.5; and (f) 4.0.

Acknowledgement

The authors thank Andrew Majda and Yakov Sinai for interesting discussions and comments, as well as two anonymous referees for insightful comments. M.G. was supported in part by the National Science Foundation. J.L. was supported in part by the National Science Foundation. S.W. was supported in part by the Office of Naval Research, by the National Science Foundation.

References

[1] G.I. Batchelor, An Introduction to Fluid Mechanics, Cambridge University Press, London, 1967.
[2] W.R. Briley, A numerical study of laminar separation bubbles using the Navier–Stokes equations, J. Fluid Mech. 47 (1971) 713–736.
[3] M. Chipot, F.B. Weissler, Some blow up results for nonlinear parabolic equation with a gradient term, SIAM J. Math. Anal. 20 (1989) 886–907.
[4] A.J. Chorin, J.E. Marsden, A Mathematical Introduction to Fluid Mechanics, Springer-Verlag, 1997.
[5] W. E, Boundary layer theory and the zero-viscosity limit of the Navier–Stokes equation, Acta Math. Sin. (Engl. Ser.) 16 (2000) 207–218.
[6] W. E, B. Engquist, Blow up of solutions of the unsteady Prandtl's equation, Commun. Pure Appl. Math. 50 (1997) 1287–1293.
[7] W. E, J.-G. Liu, Vorticity boundary condition for finite difference schemes, J. Comput. Phys. 124 (1996) 368–382.
[8] W. E, J.-G. Liu, Essentially compact schemes for unsteady viscous incompressible flows, J. Comput. Phys. 126 (1996) 122–138.
[9] M. Ghil, S. Childress, Topics in geophysical fluid dynamics: atmospheric dynamics, dynamo theory, and climate dynamics, Applied Mathematical Sciences, vol. 60, Springer-Verlag, 1987.
[10] M. Ghil, T. Ma, S. Wang, Structural bifurcation of 2-D incompressible flows, Indiana Univ. Math. J. 50 (2001) 159–180.
[11] M. Ghil, T. Ma, S. Wang, Structural bifurcation of 2-D nondivergent flows with Dirichlet boundary conditions, SIAM J. Appl. Math., 2003, submitted.
[12] D. Gilbarg, N.S. Trudinger, Elliptic Partial Differential Equations, Springer-Verlag, 1975.
[13] S. Goldstein, Modern Developments in Fluid Fynamics, vols. I and II, Dover Publications, New York, 1965.
[14] E. Grenier, Non dérivation des équations de Prandtl, Séminaire sur les Équations aux Dérivées Partielles, Ecole Polytechnique, Exp. No. XVIII, 1998, pp. 1–12.
[15] H. Johnston, J.-G. Liu, W. E, Zero viscosity limit of the flow past a cylinder, in preparation.
[16] L. Landau, E.M. Lifschitz, Fluid Mechanics, Pergamon Press, 1976.
[17] J.-G. Liu, Z. Xin, Boundary layer behavior in the fluid-dynamic limit for a nonlinear model Boltzmann equation, Arch. Rat. Mech. Anal. 135 (1996) 61–105.
[18] T. Ma, S. Wang, Dynamics of incompressible vector fields, Appl. Math. Lett. 12 (1999) 39–42.
[19] T. Ma, S. Wang, Structure of 2-D incompressible flows with the Dirichlet boundary conditions, Discrete Cont. Dyn. Syst. B 1 (2001) 29–41.
[20] T. Ma, S. Wang, A Generalized version of the Poincaré-Hopf index formula and its applications to 2-D incompressible flows, Nonlinear Anal.: Real World Applic. 2 (2001) 467–482.
[21] A.J. Majda, A.L. Bertozzi, Vorticity and Incompressible Flow, Cambridge University Press, 2001.
[22] L. Nirenberg, Topics in Nonlinear Functional Analysis, Courant Lecture Notes, New York University, 1974.
[23] O. Oleinik, On the mathematical theory of boundary layer for unsteady flow of incompressible fluid, J. Appl. Math. Mech. 30 (1966) 951–974.
[24] O.A. Oleinik, V.N. Samokhin, Mathematical Models in Boundary Layer Theory, Chapman and Hall, 1999.
[25] J. Pedlosky, Geophysical Fluid Dynamics, second ed., Springer-Verlag, New-York, 1987.
[26] L. Prandtl, Verhandlungen des dritten internationalen Mathematiker-Kongresses, Heidelberg, 1904, Leipzig, 1905, pp. 484–491.
[27] M. Sammartino, R.E. Caflisch, Zero viscosity limit for analytic solutions of the Navier–Stokes equations on a half plane. I. Existence for Euler and Prandtl equations, Commun. Math. Phys. 192 (1998) 463–491.
[28] M. Sammartino, R.E. Caflisch, Zero viscosity limit for analytic solutions of the Navier–Stokes equations on a half plane. II. Construction of the Navier–Stokes solution, Commum. Math. Phys. 192 (1998) 433–461.
[29] H. Schlichting, Boundary Layer Theory, eighth ed., Springer, Berlin-Heidelberg, 2000.
[30] L. Van Dommelen, S. Shen, The spontaneous generation of the singularity in a separating laminar boundary layer, J. Comput. Phys. 38 (1980) 125–140.
[31] C. Wang, J.-G. Liu, Analysis of finite difference schemes for unsteady Navier–Stokes equations in vorticity formulation, Numer. Math. 91 (2002) 543–576.

[32] C. Wang, J.-G. Liu, Fourth order convergence of compact finite difference solver for 2-D incompressible flow, Commun. Appl. Anal. 7 (2003) 171–191.
[33] X. Wang, R. Temam, Asymptotic analysis of oseen type equations in a channel at high Reynolds number, Indiana Univ. Math. J. 45 (1996) 863–916.
[34] X. Wang, R. Temam, Asymptotic analysis of the linearized Navier–Stokes equations in a general 2-D domain, Asymptotic Analysis 9 (1996) 1–30.
[35] Z. Xin, L. Zhang, On the global existence of solutions to the Prandtl's system, Adv. Math. 181 (2004) 88–133.